Monthly Notices
of the
ROYAL ASTRONOMICAL SOCIETY
MNRAS **456,** 1681–1699 (2016) doi:10.1093/mnras/stv2706

The abundance and colours of galaxies in high-redshift clusters in the cold dark matter cosmology

Alexander I. Merson,[1⋆] Carlton M. Baugh,[2] Violeta Gonzalez-Perez,[2] Filipe B. Abdalla,[1,3] Claudia del P. Lagos[4,5] and Simona Mei[6,7,8]

[1]*Department of Physics and Astronomy, University College London, Gower Street, London WC1E 6BT, UK*
[2]*Institute for Computational Cosmology (ICC), Department of Physics, Durham University, South Road, Durham DH1 3LE, UK*
[3]*Department of Physics and Electronics, Rhodes University, PO Box 94, Grahamstown 6140, South Africa*
[4]*European Southern Observatory, Karl-Schwarzschild-Strasse 2, D-85748 Garching, Germany*
[5]*International Centre for Radio Astronomy Research (ICRAR), M468, University of Western Australia, 35 Stirling Hwy, Crawley, WA 6009, Australia*
[6]*GEPI, Observatoire de Paris, Section de Meudon, 5 Place J. Janssen, F-92190 Meudon Cedex, France*
[7]*Université Paris Denis Diderot, F-75205 Paris Cedex 13, France*
[8]*Infrared Processing and Analysis Center, California Institute of Technology, Pasadena, CA 91125, USA*

Accepted 2015 November 17. Received 2015 November 3; in original form 2015 February 17

ABSTRACT

High-redshift galaxy clusters allow us to examine galaxy formation in extreme environments. Here we compile data for 15 $z > 1$ galaxy clusters to test the predictions from a state-of-the-art semi-analytical model of galaxy formation. The model gives a good match to the slope and zero-point of the cluster red sequence. The model is able to match the cluster galaxy luminosity function at faint and bright magnitudes, but underestimates the number of galaxies around the break in the cluster luminosity function. We find that simply assuming a weaker dust attenuation improves the model predictions for the cluster galaxy luminosity function, but worsens the predictions for the red sequence at bright magnitudes. Examination of the properties of the bright cluster galaxies suggests that the default dust attenuation is large due to these galaxies having large reservoirs of cold gas as well as small radii. We find that matching the luminosity function and colours of high-redshift cluster galaxies, whilst remaining consistent with local observations, poses a challenge for galaxy formation models.

Key words: methods: numerical – galaxies: abundances – galaxies: clusters: general – galaxies: evolution – galaxies: high-redshift – galaxies: luminosity function, mass function.

1 INTRODUCTION

Galaxy clusters are the most massive bound structures found in the Universe. Not only are clusters excellent proxies for massive dark matter (DM) haloes (and therefore a useful cosmological probe), but they are also unique sites of galaxy evolution (e.g. Kravtsov & Borgani 2012).

Over the past decade a wealth of observational data has been gathered that points towards the redshift range $z \sim 1.5$–2.5 as being a pivotal epoch in the evolutionary history of the galaxy population, with star formation, black hole accretion and galaxy mergers reaching their peak activity before being subsequently suppressed (e.g. Dickinson et al. 2003; Hopkins 2004). Similarly, observations indicate that at this epoch galaxy clusters and proto-clusters were in the process of being transformed from dynamical, merger-driven overdensities to the more relaxed systems that we see today. As such, there is mounting evidence that this redshift range marks the quenching of star formation in massive cluster galaxies and the build-up of the cluster red sequence (RS; Bower, Lucey & Ellis 1992a,b; Lidman et al. 2008; Brammer et al. 2011). However, developing a physical description of the rapid evolution of the galaxy population in clusters in this transformation phase represents a challenge for current models of galaxy formation.

The next generation of cosmological galaxy surveys, such as the *Dark Energy Survey* (DES; The Dark Energy Survey Collaboration 2005) or the European Space Agency's *Euclid* mission (Laureijs et al. 2011), are expected to observe many thousands of high-redshift galaxy clusters. However, identifying galaxy clusters in the huge volumes probed by these surveys is a difficult task fraught with systematics, especially as these surveys will be predominantly photometric. The large uncertainties inherent in photometric redshift estimation make the identification of cluster members based upon their spatial separation, as is the case for the *friends-of-friends* (Huchra & Geller 1982) and *Voroni-Delaney* methods (Marinoni et al. 2002), much more challenging (e.g. Zandivarez et al. 2014).

A more favourable approach for photometric data sets is to identify cluster members based upon whether they lie on the cluster RS in the colour–magnitude relation (CMR). Under the assumption

⋆E-mail: alexander.merson@ucl.ac.uk

that early-type galaxies dominate the cluster galaxy population and that this population follows a tight relation in colour–magnitude space, then, when imaged in two photometric bands bracketing the 4000 Å break, the cluster galaxies will be the brightest, reddest objects (Stanford, Eisenhardt & Dickinson 1998; Gladders & Yee 2000). The observational efficiency of this approach has led to it being used extensively in cluster detection (Gladders & Yee 2005; Wilson et al. 2006) and adopted in several group and cluster finding algorithms (e.g. Koester et al. 2007; Murphy, Geach & Bower 2012; Rykoff et al. 2014). As discussed in Gladders & Yee, optical and infrared imaging of local and $z > 1$ galaxy clusters indicates the universal presence of an RS (e.g. Baldry et al. 2004; Bell et al. 2004; Brinchmann et al. 2004), with many studies supporting a high formation redshift of the stellar population of $z_f \gtrsim 2$ (e.g. Ellis et al. 1997; Smail et al. 1998; Stanford et al. 1998; Ponman, Cannon & Navarro 1999; López-Cruz, Barkhouse & Yee 2004; Gladders & Yee 2005; Miller et al. 2005; Voit 2005; Mei et al. 2006a,b, 2009, 2012; Koester et al. 2007; Gilbank et al. 2008, 2011; Lidman et al. 2008; Wilson et al. 2009; Lin et al. 2012). There is, however, some observational evidence for ongoing star formation in clusters at $z \gtrsim 1$, (e.g. Hayashi et al. 2010; Brodwin et al. 2013; Fassbender et al. 2014; Mei et al. 2015).

Although using galaxy colours to identify galaxy clusters is preferable when dealing with the larger uncertainties inherent in photometric redshifts (e.g. Abdalla et al. 2011), this approach is sensitive to our understanding of the astrophysical processes governing the evolution of galaxies in cluster environments and the build-up of the RS, as well as possible biases introduced by photometric colour selections. As a result, the RS method must be tested and calibrated. At low redshift this can be done with spectroscopic data sets, but at higher redshifts, where the spectroscopic data are sparse, one must turn to using synthetic 'mock' catalogues based upon the latest galaxy formation models (Baugh 2008).

Due to their rarity, generating a population of galaxy clusters requires very large volume cosmological *N*-body simulations, which due to limitations in computational resources are typically DM only simulations. Several techniques are available for populating the haloes from *N*-body simulations with galaxies. A common approach is to use empirical methods, such as the *halo occupation distribution* (HOD; Berlind & Weinberg 2002) or *sub-halo abundance matching* (Vale & Ostriker 2004). These methods have the benefit that they are tuned using observations to ensure that the luminosity function and colour distribution of the galaxies are correct by construction. At high redshifts, however, the lack of observational data prohibits the use of such methods, though some redshift-dependent approaches have been proposed (e.g. Moster, Naab & White 2013).

Instead, *semi-analytic* galaxy formation models provide a more flexible alternative (Baugh 2006). These models use simple prescriptions to describe the various physical processes governing the evolution of the baryon content of the haloes and aim to predict the fundamental properties of galaxies, such as their stellar mass and star formation history, ab initio. Adoption of a stellar population synthesis (SPS) model, and a choice of initial stellar mass function, allows one to translate these fundamental properties into directly observable properties. Although semi-analytic models still require observational data to constrain their parameters,[1] they have been shown to make realistic predictions for the evolution of the global galaxy population out to high redshift (e.g. Lacey et al. 2011). However, given the extreme cosmic evolution of galaxy clusters, which account for only a few per cent of all mass today, making accurate predictions for the properties of high-redshift cluster galaxies remains a challenge as we shall see.

Here, we examine the predictions made by a semi-analytical galaxy formation model for the near-infrared (near-IR) photometry of galaxies in clusters at redshifts $z > 1$. Our decision to examine the statistics of clusters at this epoch in the near-infrared is motivated by the aims of the *Euclid* mission, which will provide a deep survey over 15 000 deg^2 of the sky to a photometric depth of $H \lesssim 24$. As such, *Euclid* is predicted to provide a uniformly selected sample of approximately 60 000 clusters with a signal-to-noise ratio greater than 3, with approximately 10 000 of these lying at $z > 1$ (Laureijs et al. 2011). Examining the near-IR predictions for this epoch is therefore extremely timely in the preparation for *Euclid*. The statistics that we consider are the CMR, due to its important role in cluster identification, and the cluster galaxy luminosity function (CGLF), which is one of the simplest statistics that can be made for the population of cluster galaxies.

In Section 2, we introduce the galaxy formation model and describe how we select galaxies in clusters. The set of observed clusters, which we compare with the model predictions, are introduced in Section 3. In Section 4 we compare the model predictions for the CGLF, to observational estimates between redshifts $z = 1.2$ and $z = 1.6$ and examine possible factors that might be causing the discrepancy between the observations and the model predictions. Next, in Section 5, we compare the model predictions for the CMR, of cluster galaxies with the observed one. In Section 6 we examine the effect of varying selected model parameters. Finally, we draw our conclusions in Section 7.

All synthetic and observed magnitudes have been converted to the AB system.

2 GALAXY FORMATION MODEL

In this section, we describe the galaxy formation model that we employ, starting with the *N*-body simulation used (Section 2.1) and followed by the semi-analytical model (Section 2.2). We then discuss the dust attenuation treatment used in the model (Section 2.3) and explain how we define a galaxy cluster (Section 2.4).

2.1 *N*-body simulation

The cosmological simulation that we use is a revision of the *Millennium Simulation* (Springel et al. 2005), constructed using a cosmology consistent with the 7 year results of the *Wilkinson Microwave Anisotropy Probe* (*WMAP*7; Komatsu et al. 2011). The cosmological parameters are: a baryon matter density $\Omega_b = 0.0455$, a total matter density $\Omega_m = \Omega_b + \Omega_{CDM} = 0.272$, a dark energy density $\Omega_\Lambda = 0.728$, a Hubble constant $H_0 = 100\,h\,\mathrm{km\,s^{-1}\,Mpc^{-1}}$ where $h = 0.704$, a primordial scalar spectral index $n_s = 0.967$ and a fluctuation amplitude $\sigma_8 = 0.810$. We shall refer to this simulation as the *MS-W7 Simulation* (Guo et al. 2013).

The hierarchical growth of cold DM structure is followed from redshift $z = 127$ to the present day, in a cubic volume of size $500\,h^{-1}$ Mpc on a side. Halo merger trees are constructed using particle and halo data stored at 62 fixed epoch snapshots, which are spaced approximately logarithmically in expansion factor. Details regarding construction of the halo merger trees can be found in Merson et al. (2013) and Jiang et al. (2014). The MS-W7 simulation

[1] Unlike HODs, the observational data used to constrain semi-analytic models need not be from the particular epoch of interest. Semi-analytic models can be constrained using local observations and then be used to make high-redshift predictions.

uses 2160^3 particles to represent the matter distribution, with the requirement that a halo consists of at least 20 particles for it to be resolved. This corresponds to a halo mass resolution of $M_{\rm halo,\,lim} = 1.87 \times 10^{10}\,h^{-1}\,{\rm M}_{\odot}$, significantly smaller than expected for the Milky Way's DM halo.

2.2 The GALFORM semi-analytical model

To model the star formation and merger history of galaxies we use the GALFORM semi-analytical model of galaxy formation (Cole et al. 2000). The model populates DM haloes with galaxies by using a set of coupled differential equations to determine how the various baryonic components of galaxies evolve (Baugh 2006; Benson 2010).

For the work presented here we use a development of GALFORM that accounts for the following physical processes: (i) the collapse and merging of DM haloes, (ii) the shock-heating and radiative cooling of gas inside DM haloes, leading to the formation of galactic discs, (iii) quiescent star formation in galactic discs, explicitly following the atomic and molecular gas components (Lagos et al. 2011, 2012), (iv) feedback as a result of supernovae, active galactic nuclei (AGN; Bower et al. 2006) and photo-ionization of the inter-galactic medium, (v) chemical enrichment of stars and gas, (vi) dynamical friction driven mergers of galaxies within DM haloes, capable of forming spheroids and triggering starburst events, and (vii) disc instabilities, which can also trigger starburst events.

Most of the published versions of GALFORM adopt a single Kennicutt (1983) initial mass function (IMF; see Baugh et al. 2005 for an illustration of using a top-heavy IMF in starbursts) and updated versions of SPS models from Bruzual & Charlot (1993). (See Gonzalez-Perez et al. 2014 for a comparison of coupling GALFORM with different SPS models.) By combining the star formation histories of the galaxies with the SPS models, GALFORM is able to calculate spectral energy distributions (SEDs) for the galaxies. Absolute magnitudes in a given photometric band can be obtained by integrating the SED with the corresponding frequency-dependent filter response curve. (To calculate magnitudes in the observer-frame, a frequency shift is first applied to the filter response curve.) All magnitudes and colours are total magnitudes. Apparent magnitudes are calculated using the redshift of the simulation snapshot to determine the distance modulus (see Merson et al. 2013). Note that the model magnitudes do not include any photometric uncertainties (see Ascaso, Mei & Benítez 2015 for a discussion of the impact of photometric errors on the CMR).

GALFORM is able to track the global metallicity for the stars, as well as the hot and cold gas in the galaxy. Chemical enrichment is modelled using the instantaneous recycling approximation, with an effective yield and a recycled fraction that depend upon the choice of IMF. The yield is modified accordingly by metal ejection and feedback and hence is a function of the depth of the potential well of the galaxy. The rate at which gas is ejected from the galaxy due to supernovae explosions, $\dot{M}_{\rm eject}$, is given by

$$\dot{M}_{\rm eject} = \left(\frac{v_{\rm hot}}{v_{\rm disc}}\right)^{\alpha_{\rm hot}} \dot{M}_{\star}, \tag{1}$$

where $v_{\rm disc}$ is the circular velocity of the galaxy disc at the half-mass radius, $\dot{M}_{\star}$ is the star formation rate and $\alpha_{\rm hot}$ and $v_{\rm hot}$ are free parameters that govern the strength of supernovae feedback.

In GALFORM, feedback due to AGN is implemented in haloes that are undergoing quasi-static cooling, where, at fixed radius, the cooling time of the hot halo gas, $\tau_{\rm cool}$, exceeds the dynamical free-fall time of the gas, $\tau_{\rm ff}$. Therefore, feedback due to AGN can only occur when the condition,

$$\left.\frac{\tau_{\rm ff}}{\tau_{\rm cool}}\right|_{r=r_{\rm cool}} < \alpha_{\rm cool}, \tag{2}$$

is satisfied, where $\alpha_{\rm cool}$ is a free parameter. This condition is evaluated at the cooling radius, $r_{\rm cool}$, which is defined, for a halo of a given age, as the radius at which the hot gas has only just had sufficient time to cool and collapse on to the galactic disc. Reducing the value of $\alpha_{\rm cool}$ raises the minimum halo mass at which a quasi-static halo is established, thus allowing star formation to continue for longer in more massive haloes.

The free parameters in the Gonzalez-Perez et al., model were calibrated to reproduce the b_J- and K-band luminosity functions at $z = 0$ as well as to predict a reasonable evolution for the rest-frame K-band and UV luminosity functions. We stress at this point that this model has not been explicitly constrained using any observations of high-redshift clusters.

Overall, the GALFORM model is able to make predictions for numerous galaxy properties, including luminosities over a substantial wavelength range extending from the far-UV through to the sub-millimetre. However, matching precisely the observed colour distribution of galaxies in the local Universe remains difficult for semi-analytical models (e.g. Font et al. 2008; González et al. 2009; Guo et al. 2011).

2.3 Modelling dust attenuation

The attenuation by dust of the starlight from galaxies is modelled in GALFORM using a physically motivated method based upon the results of the radiative transfer code of Ferrara et al. (1999). The method assumes the dust to be distributed in dense molecular clouds embedded in a diffuse component. In this model the dust attenuation varies self-consistently with other galaxy properties, such as size, gas mass and metallicity, which are predicted by GALFORM (see also Fontanot et al. 2009a; Fontanot & Somerville 2011). The V-band optical depth when looking face-on through the centre of a galaxy, $\tau_{\rm V}^{0}$, is assumed to be

$$\tau_{\rm V}^{0} \propto \frac{M_{\rm cold} Z_{\rm cold}}{r_{\rm disc}^{2}}, \tag{3}$$

where $M_{\rm cold}$ is the mass of cold gas in the galaxy (both atomic and molecular), $Z_{\rm cold}$ is the metallicity of the cold gas content of the galaxy and $r_{\rm disc}$ is the radius of the galactic disc. Given an extinction law, the Ferrara et al. (1999) model provides dust attenuation factors as a function of wavelength, galaxy inclination, the ratio of bulge to disc radial dust scale length, $r_{\rm e}/h_R$, the ratio of dust to stellar vertical scale heights, $h_{z,\,\rm dust}/h_{z,\,\rm stars}$, and $\tau_{\rm V}^{0}$ (see Cole et al. 2000 and Gonzalez-Perez et al. 2014 for further details).

2.4 Cluster galaxy selection

When comparing the semi-analytic predictions to the observational estimates, we consider clusters of galaxies to be hosted by dark matter haloes with mass, $M_{\rm halo}$,

$$M_{\rm halo} \geqslant 1.2 \times 10^{14}\,h^{-1}\,{\rm M}_{\odot}. \tag{4}$$

This value is chosen as a compromise to ensure that we have a sufficiently large sample of haloes that are massive enough to adequately represent our set of observed clusters. After imposing the halo mass limit we are left with 43 haloes at $z \sim 1.4$, 98 haloes at $z \sim 1.2$ and 10 haloes at $z \sim 1.6$. Cluster member galaxies are then

Table 1. High-redshift observational galaxy cluster data sets used for comparison with model predictions. Columns show: (i) reference and cluster ID, (ii) estimated cluster redshift, (iii) photometry available, (iv) aperture used to identify cluster members, (v) estimated mass of cluster from X-ray measurements, (vi) estimated mass of cluster from weak lensing measurements. Cluster-mass estimates are provided where known, with values converted to units of $10^{14}\,h^{-1}\,\mathrm{M}_{\odot}$, using the values of h specified by the original authors. Note that cluster RX J0848+4453 is listed twice.

Cluster	Cluster redshift	Photometry	Aperture (arcsec)	X-ray mass ($10^{14}\,h^{-1}\,\mathrm{M}_{\odot}$)	Lensing mass ($10^{14}\,h^{-1}\,\mathrm{M}_{\odot}$)
Mei et al. (2006b)					
RX J0849+4452	1.26	i_{775}, z_{850}	120	2.0 ± 1.0^{a}	$3.08^{+0.78\,b}_{-0.63}$
RX J0848+4453	1.27	i_{775}, z_{850}	120	0.96 ± 0.69^{a}	$2.2^{+0.7\,b}_{-0.6}$
Strazzullo et al. (2006)					
RDCS J0910+5422	1.106	H_{160}, K	73	2.1 ± 1.3^{a}	$3.5^{+0.8\,b}_{-0.7}$
RDCS J1252.9−2927	1.237	H_{160}, K	59	1.11 ± 0.24^{a}	$4.8^{+0.9\,b}_{-0.7}$
RX J0848+4453	1.273	H_{160}, K	47	0.96 ± 0.69^{a}	$2.2^{+0.7\,b}_{-0.6}$
Hilton et al. (2009)					
XMMXCS J2215.9−1738	1.46	z_{850}, J,K	153[c]	$1.4^{+0.36\,b}_{-0.42}$	$3.0^{+2.1\,b}_{-1.2}$
Strazzullo et al. (2010)					
XMMU J2235−2557	1.39	z_{850}, H_{160}, J, K	83	$4.3^{+1.0\,b}_{-0.8}$	$5.1^{+1.2\,b}_{-1.0}$
Snyder et al. (2012)					
ISCS J1426.1+3403	1.136	H_{160}, I_{814}	122	–	–
ISCS J1426.5+3339	1.163	H_{160}, I_{814}	122	–	–
ISCS J1434.5+3427	1.243	i_{775}, H_{160}	120	–	$1.8^{+1.6\,b}_{-0.8}$
ISCS J1429.3+3437	1.262	z_{850}, H_{160}	120	–	$3.8^{+1.7\,b}_{-1.1}$
ISCS J1432.6+3436	1.349	z_{850}, H_{160}	119	–	$3.7^{+1.8\,b}_{-1.2}$
ISCS J1433.8+3325	1.369	z_{850}, H_{160}	119	–	–
ISCS J1434.7+3519	1.372	z_{850}, H_{160}	119	–	$2.0^{+2.1\,b}_{-1.0}$
ISCS J1438.1+3414	1.413	z_{850}, H_{160}	119	$2.2^{+3.7\,b}_{-1.0}$	$2.2^{+1.8\,b}_{-1.0}$
Fassbender et al. (2014)					
XDCP J0044.0−033	1.58	J, K, i, V	30	2.1	–

Notes. [a]M_{500} estimate from Ettori et al. (2004).
[b]M_{200} estimate from Jee et al. (2011).
[c]Based upon maximum radial distance quoted in table 1 of Hilton et al. (2009)

taken to be those galaxies sharing a common host dark matter halo. Additionally, we place an aperture of 120 arcsec by first assuming an observer placed at infinity, viewing the haloes along the Cartesian Z-axis of the simulation box. We use the positions of galaxies labelled by GALFORM as being central galaxies, which are located at the centre of mass of the most massive sub-halo of a halo, as the positions of the halo centres. We then apply the aperture using the projected distances between the galaxies and the halo centre. The effect of our choices for the halo mass limit and aperture size, as well as our method for modelling dust attenuation, is discussed further in Section 4.2.

We stress that no colour selection is applied when selecting the GALFORM cluster galaxies and that, since we know the halo membership of the galaxies, the model predictions do not include contamination from foreground or background interlopers. For this work we are therefore examining the properties of model galaxies that truly are cluster galaxies, i.e. are hosted by cluster-mass haloes selected according to our threshold of $M_{\mathrm{halo}} \geq 1.2 \times 10^{14}\,h^{-1}\,\mathrm{M}_{\odot}$. An assessment of the effect of member incompleteness and interlopers, where cluster galaxies are selected according to their colours, is left for future work.

3 OBSERVATIONAL DATA SETS

Here we briefly introduce the observational data sets against which we will compare the model predictions.

Observations of clusters at high redshift, $z > 1$, are still limited to of the order of a few tens of clusters, often with masses exceeding $10^{14}\,h^{-1}\,\mathrm{M}_{\odot}$. Here, we consider a compilation of clusters at redshifts between $z \sim 1.2$ and $z \sim 1.6$, for which multi-band photometry is available. In particular, we focus on clusters for which photometry is available such that they could be identified by the *Euclid* mission. The clusters that we consider are listed in Table 1.

Typically, the colours used to examine cluster galaxies are chosen such that the pairs of photometric bands bracket the redshifted 4000 Å break, the strength of which is typically used as a proxy for the age of a galaxy and as a way of distinguishing passively evolving galaxies from those that are undergoing star formation when combined with other indexes (Kauffmann et al. 2003; Kriek et al. 2006, 2011), as illustrated in Fig. 1 for two synthetic galaxies at $z = 1.4$. At $z \sim 1.2$ the 4000 Å break is shifted to 8800 Å, which lies between the i and z bands, whereas at $z \sim 1.4$ the 4000 Å break, now shifted to 9600 Å, is bracketed by the z and J bands. At $z \sim 1.6$ the 4000 Å break is shifted to 10 400 Å and is still bracketed by the z and J bands.

For the majority of the clusters, mass estimates are available. In Table 1 we provide M_{200} and M_{500} mass estimates from Ettori et al. (2004) and Jee et al. (2011). In many cases the mass estimates from gravitational lensing are larger than the mass estimates based upon the X-ray emission from the cluster, which is likely to be due to projection effects in the lensing estimate. However, X-ray mass estimates are also uncertain due to the limitations in our understanding of the conditions in X-ray gas (e.g. Angulo et al. 2012).

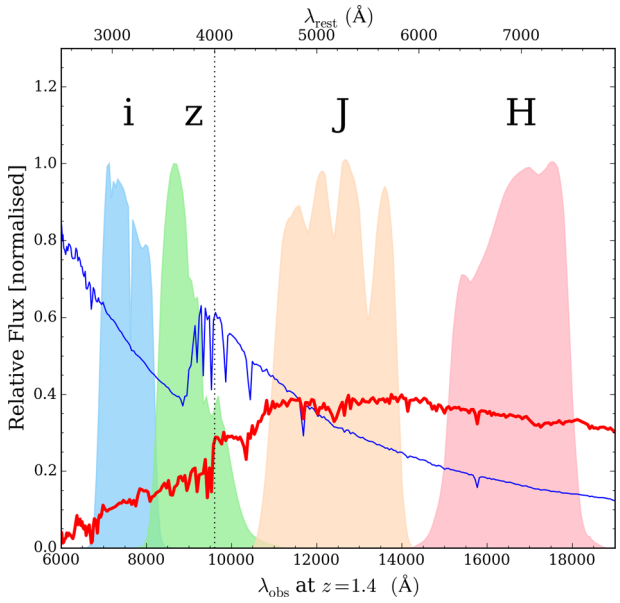

Figure 1. Examples of intrinsic spectra for two synthetic galaxies at redshift $z = 1.4$, over-plotted with transmission profiles for the i, z, J and H bands, as shown by the shaded regions. No dust attenuation is considered. Both of the galaxies were assumed to undergo a single instantaneous burst of star formation, one 300Myr ago (thin blue line) and the other 3 Gyr ago (thick red line), prior to $z = 1.4$. (Both galaxies are assumed to have a metallicity of $Z = 0.008$.) The spectra were generated using the PEGASE.2 code (Fioc & Rocca-Volmerange 1999), assuming a Kennicutt (1983) IMF. The dotted, vertical line indicates the rest-frame wavelength of 4000 Å.

In the remainder of this section we provide further details on each of the galaxy cluster data sets.

(i) *Mei et al. (2006b)*: Mei et al., present i_{775} (F775W) and z_{850} (F850LP) observations of the clusters RX J0849+4452 and RX J0848+4453, which together make up the Lynx Supercluster, located at $z \sim 1.2$. Applying the colour selection $0.8 < (i_{775} - z_{850}) < 1.1$, the flux selection $21 < z_{850} < 24$ and an aperture selection of 120 arcsec, left 40 galaxies, of which 14 are confirmed cluster members and 26 are cluster member candidates. Galaxy colours were measured within the effective radii of the galaxies. Mei et al., assumed reddening due to dust to be described by a Calzetti et al. (2000) extinction law of $E(B - V) = 0.027$ with $A_{i_{775}} = 0.054$ and $A_{z_{850}} = 0.040$.

(ii) *Strazzullo et al. (2006)*: Strazzullo et al., present K_s-band imaging for the clusters RDCS J0910+5422 ($K_s < 21.5$) and RDCS J1252.9−2927 ($K_s < 24.5$), as well as H_{160} (F160W) imaging for RX J0848+4453 ($H_{160} < 25$). They present an estimate for the CGLF for each cluster, as well as a composite estimate for all three of the clusters. The apertures applied are listed in Table 1.

(iii) *Hilton et al. (2009)*: Hilton et al., present J- and K_s-band photometry, along with $z_{850} - J$ and $z_{850} - K_s$ colour information, for 64 galaxies selected as members of the cluster XMMXCS J2215.9−1738. The radial distance of the galaxies relative to the cluster X-ray source position extends out to 922 kpc. Spectroscopic redshifts are obtained for 24 of these galaxies. The photometry was corrected for Galactic extinction using the dust emission maps of Schlegel, Finkbeiner & Davis (1998).

(iv) *Strazzullo et al. (2010)*: Strazzullo et al., present multi-wavelength data for the cluster XMMU J2235−2557, one of the most massive virialized structures found beyond $z \sim 1$. They present estimates for the CGLF of the cluster in z_{850}, H_{160} and K_s, with 10σ completeness limits of $z_{775} < 25.3$, $H_{160} < 25$ and $K_s < 23$. They also apply an aperture and select only those galaxies within 83 arcsec of the cluster centre. The photometry was corrected for Galactic extinction using the dust emission maps of Schlegel et al. (1998). Strazzullo et al., argue that for their data set the population of brightest galaxies in the inner region of the cluster can be considered to be quite well established, with about seventy per cent of these galaxies having measured spectroscopic redshifts.

(v) *Snyder et al. (2012)*: Snyder et al., present *Hubble Space Telescope* follow up observations of clusters selected from the *Spitzer*/IRAC Shallow Cluster Survey (ISCS; Eisenhardt et al. 2008). They provide photometry for these clusters in the H_{160} band and one of the I_{814}, i_{775} or z_{850} bands. They report that the detection catalogues for each cluster are more than 90 per cent complete for $H_{160} < 23.5$. To identify cluster galaxies lying on the RS, they subtract from the colour of each galaxy a fiducial evolved CMR model for the Coma cluster and apply a selection based upon the residual. Reddening due to dust is assumed to be small, approximately $E(B - V) \lesssim 0.06$.

(vi) *Fassbender et al. (2014)*: Fassbender et al., present VLT/HAWK-I J- and K_s-band observations of the cluster XDCP J0044.0−033, complemented with the V and i bands from *Subaru* archival imaging. They report that their observations are 100 per cent complete down to $J \lesssim 23.9$ and $K_s \lesssim 23.8$. To maximize the signal-to-noise ratio of the cluster members to the interlopers, Fassbender et al., apply an aperture of 30 arcsec. They estimate that the galaxies within this radius are 90 per cent cluster-associated.

4 THE CLUSTER GALAXY LUMINOSITY FUNCTION

In this section we compare observational estimates for the CGLF, which describes the number of galaxies per cluster as a function of apparent magnitude, with the predictions from our reference model. We stress again that for the model predictions, knowledge of the halo membership of the galaxies means that we can simply select cluster galaxies using a halo mass selection and that no further colour selections are imposed. The observational estimates and semi-analytical predictions for the z-band CGLF are shown in Fig. 2, the H-band CGLF in Fig. 3 and the K-band CGLF in Fig. 4. The observational estimates are shown by the various data points, whilst the model predictions are indicated by the solid lines (with shaded regions indicating the Poisson uncertainties).

4.1 Observational estimates

In Figs 2–4 we show observational estimates for the CGLF from Strazzullo et al. (2006, 2010) and Fassbender et al. (2014), as well as our estimates based upon the data sets of Mei et al. (2006b), Hilton et al. (2009) and Snyder et al. (2012).

Strazzullo et al. (2006, 2010) estimate the CGLF for their galaxy cluster sample by using a reference field, down to an equivalent photometric depth or deeper, to statistically remove the contribution from background galaxies, which is known to bias CGLF estimates (Andreon, Punzi & Grado 2005), particularly at bright magnitudes where the statistics are typically quite poor. The CGLF is estimated by subtracting the counts in the reference field (normalized to the solid angle of the cluster) from the counts in the cluster field. The uncertainties on the CGLFs estimated by Strazzullo et al. (2006, 2010) are Poisson, with both clusters and possible background field interlopers summed in quadrature. The limits on the excess counts are determined based upon the upper and lower limits on the number of sources with a spectroscopic redshift or a photometric redshift

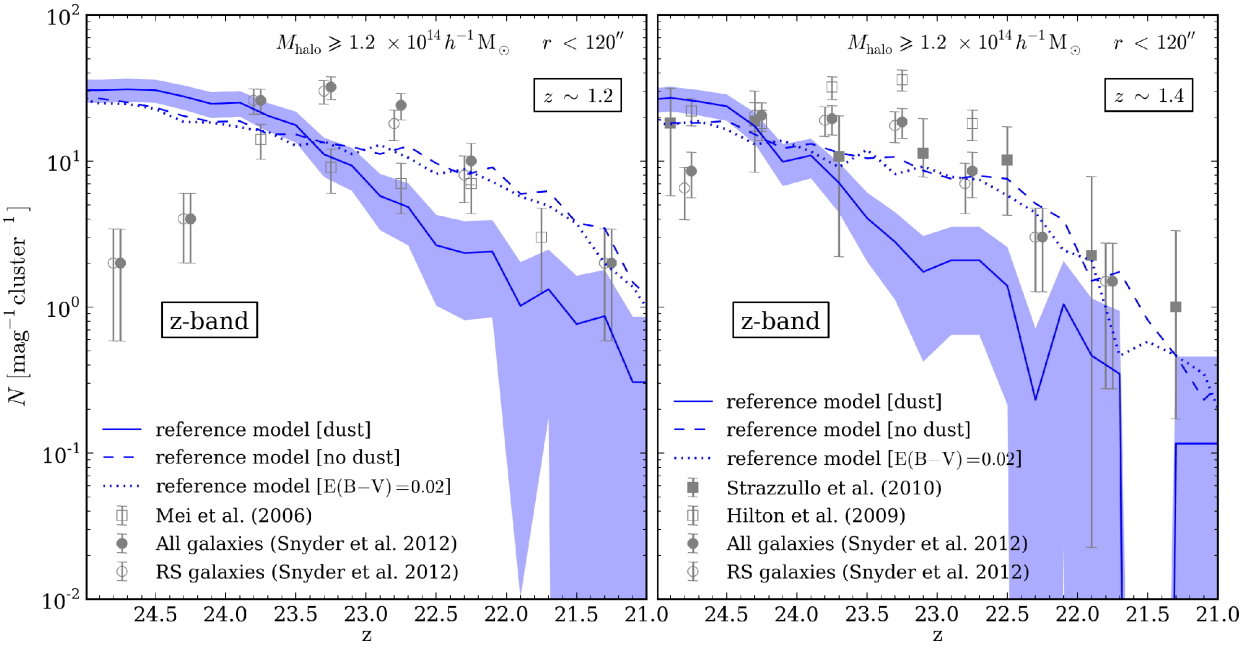

Figure 2. z-band CGLF at redshifts $z \sim 1.2$ (left) and $z \sim 1.4$ (right). The blue, solid line shows the predicted CGLF for the reference model, with dust attenuation. The shaded region indicates the Poisson uncertainty on this prediction. The dashed line shows the prediction for the reference model with no dust attenuation applied, i.e. using the fluxes intrinsic to the galaxies. The dotted line shows the prediction for the reference model when a dust attenuation similar to a Calzetti et al. (2000) extinction law with E(B − V) = 0.02 is assumed. All model predictions correspond to the CGLF for all cluster galaxies within an aperture of 120 arcsec, hosted by dark matter haloes of $M_{\rm halo} \geq 1.2 \times 10^{14}\,h^{-1}\,{\rm M}_{\odot}$. Observational estimates of the luminosity functions are indicated by various data points.

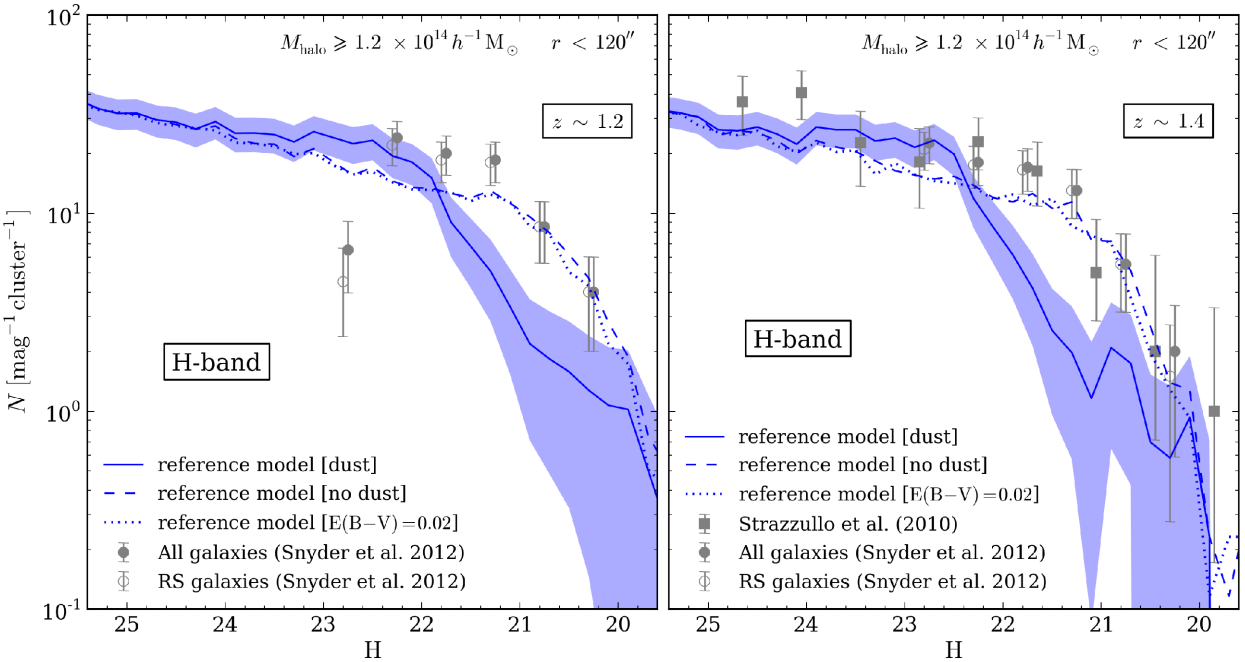

Figure 3. H-band CGLF at redshifts $z \sim 1.2$ (left) and $z \sim 1.4$ (right). All model predictions correspond to the CGLF for all cluster galaxies, with galaxies selected in the same way as in Fig. 2. Observational estimates of the luminosity functions are indicated by various data points.

within 3σ of the cluster redshift. Strazzullo et al. (2006) argue that the background contamination from lensed galaxies magnified by the cluster itself is small. They conclude that their estimate for the CGLF is consistent with previous determinations at similar or lower redshifts. Fassbender et al., adopt the same selection procedure as Strazzullo et al. (2006) when estimating the $z \sim 1.6$ K-band CGLF.

For the data sets of Mei et al., Hilton et al., and Snyder et al., we have made simple estimates for the CGLF by counting all of the galaxies regarded as being cluster members by the original authors. From the Mei et al., data we estimate the z-band CGLF at $z \sim 1.2$. From the Hilton et al., data we estimate the z- and K-band CGLFs at $z \sim 1.4$. From the Snyder et al., data we estimate

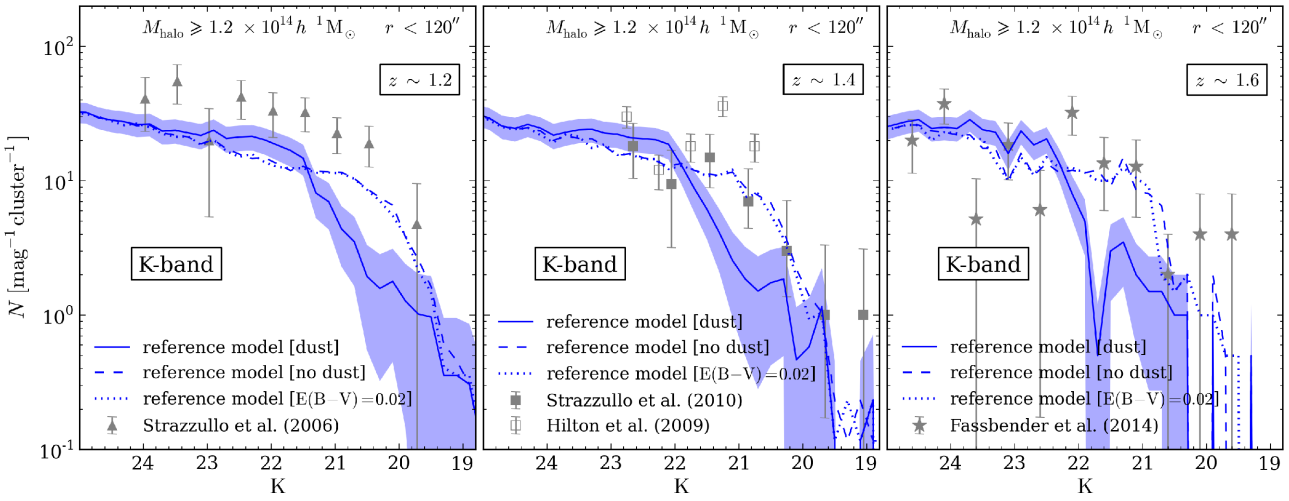

Figure 4. K-band CGLF at redshifts $z \sim 1.2$ (left), $z \sim 1.4$ (middle) and $z \sim 1.6$ (right). All model predictions correspond to the CGLF for all cluster galaxies, with galaxies selected in the same way as in Fig. 2. Observational estimates of the luminosity functions are indicated by various data points.

the z- and H-band CGLFs at $z \sim 1.2$ and $z \sim 1.4$. We apply no further selection beyond those placed originally by the authors and provide simple Poisson uncertainties on these counts. As such, our estimated uncertainties on these observational luminosity functions may well be underestimated and our CGLF estimates may be biased by membership incompleteness.

At $z \sim 1.4$, in the z and H bands, we compare our estimates for the CGLF to the estimates from Strazzullo et al. (2010), though these are for a slightly more massive cluster and adopt a smaller aperture when selecting the member galaxies (as we demonstrate in Section 4.2.1, changing the aperture size has a greater impact at the faintest magnitudes). We find that our CGLF estimates from the Snyder et al., data are consistent within error with the estimates from Strazzullo et al. When constructing their data set, Snyder et al., identified galaxies as cluster members based upon the likelihood of the galaxy lying on the cluster RS. For a subset of the galaxies these authors were able to confirm that they indeed are on the RS of the clusters. In Figs 2 and 3 we plot the Snyder et al., estimate for the CGLF using only the confirmed RS galaxies and can see that this is in excellent agreement with the estimate using the full Snyder et al., data set, suggesting that our CGLF estimates are not being significantly biased by possible interloping non-member galaxies.

At $z \sim 1.2$, there are no existing estimates of the CGLF in the H or z bands against which to compare ours. In these bands our estimates from the Snyder et al., data set show a bright-end fall off similar in shape to the CGLF estimates at $z \sim 1.4$. At the faintest magnitudes, however, the CGLFs show a down-turn. Snyder et al., report 5σ detection limits of 26.0–26.3 in the z band and 24.4–24.8 in the H band, with 90 per cent completeness at H $\sim$ 23.5. It is possible therefore that the observed down-turns may be a result of incompleteness. When determining their samples of cluster galaxies, Snyder et al., place a selection limit of H $\sim$ 22–23, determined for each cluster by evolving the characteristic brightness of the Coma cluster to the redshift of each cluster. This selection may also be contributing to the down-turns.

In the z-band, our estimate for the CGLF from the Mei et al., shows good agreement with the Snyder et al., estimate for magnitudes bright-wards of z $\sim$ 22.2. Faint-wards of this value, however, the estimates diverge. We note that these estimates are based upon galaxies from only one or two clusters, so discrepancies are indeed possible due to cosmic variance across the cluster populations. Another possible cause could be due to the i − z colour selection that Mei et al., place in order to identify early-type galaxies. We note, however, that the uncertainties on our CGLF estimates are simple Poisson errors and so may well be underestimates of the true uncertainties. If this is the case, then it is possible that our estimates for these two datasets are consistent within error.

Our estimates for the z- and K-band CGLFs from the Hilton et al., data set are generally consistent with the other estimates presented, though there are one or two bins for which the counts are higher than the other estimates, for example at z $\sim$ 23.2 and K $\sim$ 21.2. Just under two-thirds of galaxies in the Hilton et al. data have photometric redshifts only and so this variation could be caused by interlopers. In addition, variation due to cosmic variance between CGLF measurements for different clusters would be expected.

4.2 Semi-analytical predictions

The predictions for the CGLF from our reference GALFORM model are shown in Figs 2–4 by the solid blue lines, with shaded regions indicating the Poisson uncertainties. These predictions correspond to the CGLF for *all* cluster galaxies, i.e. all galaxies in haloes with mass $M_{\rm halo} \geq 1.2 \times 10^{14} h^{-1}{\rm M}_{\odot}$, within a projected aperture of $r < 120$ arcsec.

There is a large discrepancy between the model predictions and the observational estimates around the knee of the CGLF. This discrepancy is most obvious in the H- and K-band CGLF comparisons, though it is still apparent in the z-band CGLF, particularly at $z \sim 1.4$. In the brightest and faintest magnitude bins, however, the model predictions for the CGLF are broadly consistent with the observational estimates.

In the H and K bands, the model predictions for the CGLF show a faint-end slope that is quite flat, in agreement with the faint-end slope seen in the observations. In the K-band, however, the normalization of the slope in the model predictions is lower than that of the observations, particularly at $z \sim 1.2$.

We now consider three factors that could affect our comparison with cluster data, particularly our estimation of the CGLF. These are: the size of the aperture we apply to the halo (Section 4.2.1), our choice of halo mass limit applied to the model (Section 4.2.2) and our modelling of attenuation due to dust (Section 4.2.3).

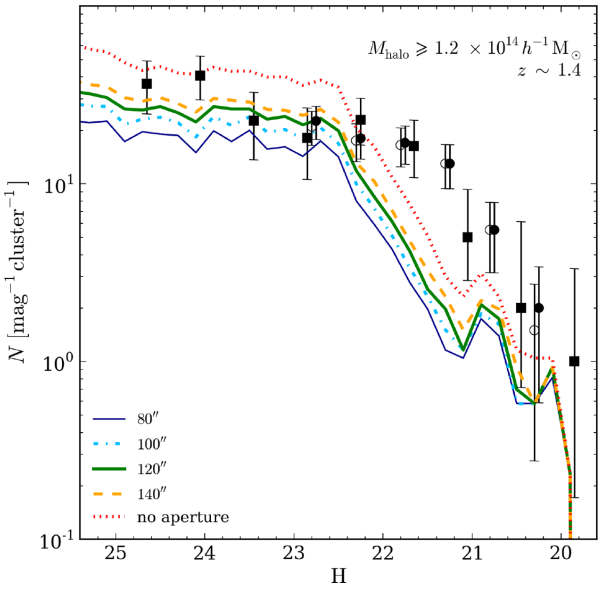

Figure 5. H-band CGLFs at $z \sim 1.4$ as predicted by GALFORM assuming different apertures for selecting the member galaxies of each halo, as indicated in the legend. For each choice of aperture a halo mass limit of $M_{\rm halo} \geq 1.2 \times 10^{14}\,h^{-1}\,{\rm M}_{\odot}$ was adopted. The data points are the same as in the right-hand panel of Fig. 3.

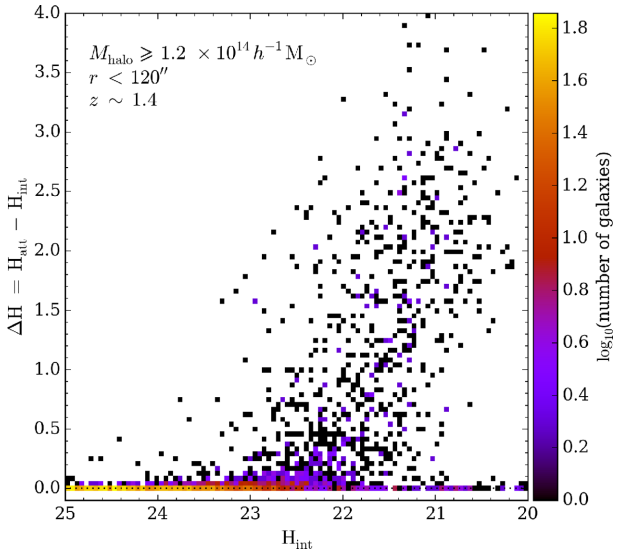

Figure 6. Difference in GALFORM H-band attenuated magnitudes, $\rm H_{att}$, and H-band intrinsic magnitudes, $\rm H_{int}$, as a function of intrinsic magnitude. (The default dust attenuation calculation is assumed.) The colour bar indicates the number of galaxies in each pixel. The redshift, as well as the halo mass and aperture used to select the GALFORM galaxies, are shown in top right of the panel.

4.2.1 *Aperture size*

We select the GALFORM cluster galaxies using an aperture size of $r < 120$ arcsec, which is consistent with the apertures placed by Mei et al. (2006b) and Snyder et al. (2012). Given the cosmology used in the MS-W7 simulation, an aperture of 120 arcsec corresponds approximately to a distance of $500\,h^{-1}$ kpc at $z \sim 1.4$. Varying the aperture size will change the number of satellite galaxies that are included. We must therefore examine how a change in aperture size affects our estimates of the CGLF.

In Fig. 5 we plot the predictions for the reference model for the H-band CGLF at $z \sim 1.4$ when keeping the halo mass limit fixed and allowing the aperture size to vary. The variation of the aperture size induces a change in the abundance of cluster members, particularly for the faintest magnitude bins where a change in the aperture size will lead to different numbers of faint satellite galaxies being selected. This change in the abundance, typically within a factor of two, is consistent with observational uncertainties. All of the apertures we consider correspond to distances smaller than the virial radius of a typical cluster-sized dark matter halo and so remove the most distant satellites from the comparison such that we are comparing only the cores of the clusters. At brighter magnitudes, $\rm H \lesssim 21.5$, the change in the abundance becomes smaller due to the increasing number of bright, central galaxies, which will always be selected. If we remove the aperture altogether then we see an increase of approximately a factor of two in the abundance of cluster members with $\rm H \gtrsim 21.5$, as all of the most distant satellites are now included (shown by the red line in Fig. 5).

From Fig. 5 we can see that an aperture of 120 arcsec is consistent with many of the aperture choices in Table 1 and provides a suitable match to the counts just faint-wards of the break in the CGLF.

4.2.2 *Halo mass limits*

We select cluster galaxies in GALFORM as galaxies hosted by haloes above a threshold mass of $1.2 \times 10^{14}\,h^{-1}\,{\rm M}_{\odot}$. Using a fixed aperture of 120 arcsec we find that variation of the halo mass limit between $1.0 \times 10^{14}\,h^{-1}\,{\rm M}_{\odot}$ and $1.8 \times 10^{14}\,h^{-1}\,{\rm M}_{\odot}$ produces a negligible change in predicted H-band CGLF at $z \sim 1.4$. (Examination of larger halo masses is not possible due to the limited volume of the MS-W7 simulation.) We find that the choice of halo mass limit has a negligible effect on the CGLF.

4.2.3 *Attenuation due to dust*

The dust content of a galaxy can have a drastic effect upon the observed colour of the galaxy. In Figs 2–4 we compare the model CGLF, both with and without dust attenuation, with the observations. In the reference model dust attenuation has a large impact around the knee of the CGLF. At the knee of the CGLF the reference model is about a factor of 4.5 below the observations. The observed CGLF can be reproduced if instead we consider a model without dust attenuation. However, such a model predicts an unrealistic luminosity function at $z = 0$, as we shall discuss later.

To help understand this result, we compare the intrinsic and attenuated magnitudes of the GALFORM galaxies in our reference model. We define the difference,

$$\Delta{\rm M} = {\rm M_{att.}} - {\rm M_{int.}}, \tag{5}$$

where $\rm M_{int}$ is the intrinsic, dust-free magnitude of a GALFORM galaxy and $\rm M_{att.}$ is the magnitude of this galaxy attenuated using the dust model described in Section 2.3. In Fig. 6 we plot the difference between these two magnitudes as a function of H-band intrinsic magnitude. The majority of galaxies display very little dust attenuation and so have a negligible difference between their intrinsic and attenuated magnitudes.

There are, however, a small number of galaxies, with intrinsic magnitudes between $21 < \rm H_{int.} < 23$ that display dust attenuation larger than one magnitude. If we examine again the H-band CGLF at $z \sim 1.4$ (right-hand panel of Fig. 3), we can see that this magnitude range corresponds approximately to the knee of the CGLF,

where the maximum discrepancy between the model and the observations occurs. For magnitudes outside this range, the attenuation is minimal. Hence, the size of the attenuation applied in our reference model is not constant with magnitude, unlike, for example, the simple Calzetti et al. (2000) fitting formula that is often applied to low-redshift star-forming galaxies. With our reference attenuation calculation, the large dust attenuation in the brightest galaxies causes these galaxies to be shifted out of the brightest magnitude bins and to pile up in the magnitude bins faint-wards of the characteristic magnitude. Although these galaxies constitute only of the order 5–10 per cent of galaxies with $H_{att.} < 25$ for example, the rapidly declining number of galaxies in the brightest bins means that this magnitude shift has a significant impact upon the CGLF.

As a final demonstration that these highly dust attenuated galaxies are the cause of the discrepancy between the model CGLF and the observations, we calculate again the CGLF for our reference model but now assume a weaker dust attenuation, similar to a Calzetti et al. (2000) extinction law with $E(B-V) = 0.02$. The resulting CGLF predictions are shown as blue dotted lines in Figs 2–4. In each instance, we see that weakening the attenuation in this way leads to a much better agreement between the model and the observations.

5 THE CLUSTER COLOUR–MAGNITUDE RELATION

Having examined the abundance of semi-analytical cluster galaxies, we now consider their colours. Specifically, we consider the CMR. In the CMR the RS is often used observationally to detect clusters as it is expected to be dominated by early-type cluster members. It is desirable to examine the model predictions for the RS as any discrepancy between the model and observations could, for example, impact upon the calibration of cluster-finding algorithms for next-generation surveys such as *Euclid*.

5.1 Red sequence fitting

To describe the location of the model RS, we use linear regression[2] to fit the optimized slope, s, and zero-point, $c_{22.5}$, for the relation,

$$c = s(m - 22.5) + c_{22.5}, \quad (6)$$

where m is the galaxy magnitude, e.g. H, and c is the corresponding colour, e.g. z − H. Since the RS is expected to be dominated by passively evolving galaxies and since GALFORM is able to provide us with values for the star formation rates of galaxies, as well as which haloes they belong to, we are able to fit an RS using just those galaxies that are passively evolving and reside in haloes above our specified halo mass threshold. Therefore, we stress that this is not meant to mimic observational methods for determining the RS, but simply to provide an estimate of the RS predicted by the model. To determine the passively evolving cluster galaxies, we apply a cut in instantaneous specific star formation rate (sSFR) and fit to only those galaxies that satisfy $\log_{10}(\mathrm{sSFR/Gyr^{-1}}) \leq -1$, which provides a reasonable distinction between actively star-forming and passively evolving galaxies in observational data (e.g. Williams et al. 2009) and hydrodynamical simulations (e.g. Romeo et al. 2008; Furlong et al. 2015). We therefore regard the fit to the passively evolving galaxies as our measure of the true RS predicted by the model, i.e. the RS of those cluster galaxies that are truly 'red and dead'. Note that in addition to the sSFR cut, we also select only those galaxies brighter than 25th magnitude in the appropriate band (z, J, H or K).

The fits to the passively evolved cluster galaxies provide an excellent description of the model RS down to 25th magnitude, as evident from Figs 7 and 8 where the fits to the passive RS are shown by the red, dashed lines. In these figures the grey-scale pixels show the distribution of all cluster galaxies in the model, passive and star-forming, normalized by the number of clusters (i.e. the number of haloes above the halo mass threshold). In each case the distribution is dominated by a clear and well-defined RS, especially at faint magnitudes, with very little indication of a blue cloud.

At bright magnitudes the model RS appears to display a prominent plume of galaxies with colours extending redwards above the RS. This plume is visible in many of the colour-spaces that we consider, in particular i − H, z − H and J − K. As we shall see in Section 5.3, the galaxies in the plume are star-forming and so are not identified by our sSFR selection. As such, they are not included in the fitting and do not bias the fits to the slope or the zero-point. In contrast, simply fitting the RS to a straight-forward flux-selected sample, i.e. without selecting just the passively evolving galaxies, would lead to biased fits. The results of the fits, i.e. the slope and intercept, as well as their corresponding uncertainties, are provided in Table 2.

5.2 Comparison with observed clusters

We now compare the GALFORM prediction for the cluster CMR with observational measurements at $z > 1$. In Figs 7 and 8 we show the colours of the observed cluster galaxies on top of the GALFORM predictions, shown by the grey-scale pixels. In addition, we show as a red, dashed line the fit to the passively evolving RS. The distribution of GALFORM cluster galaxies appears to be qualitatively in good agreement with the observations for each of the colour–magnitude spaces that we consider. In each instance the model RS is qualitatively in good agreement with observations. For all cases in Figs 7 and 8, the scatter in the distribution of colours from GALFORM is consistent with or smaller than the spread in the observations, though we must recall that no photometric errors are included in the model predictions.

Comparing our estimates for the slope and zero-point (see equation 6) of the model RS with fits available for the observed clusters, we find a reasonable agreement for the longer-wavelength colours, particularly for the zero-point estimates. For example, our fit to the RS in z − J is consistent with the fit from Hilton et al. (2009) who estimated a slope of -0.049 ± 0.062 and a zero-point of 1.335 ± 0.046. For the clusters ISCS J1433.8+3325, ISCS J1432.6+3436, ISCS J1434.7+3519 and ISCS J1438.1+3414, Snyder et al., determine a range of values for the z − H zero-point. Taking the mean of these values and adding the uncertainties in quadrature give an estimate of 1.78 ± 0.09, which is consistent within 1σ with our z − H fit. For i − z, our fit to the RS zero-point is close to the fit of Mei et al. (2006b), who found a zero-point of 0.99 ± 0.01. Our fit to the slope, however, is shallower than their fit of -0.031 ± 0.012.

5.3 Trends in galaxy properties

We conclude our analysis of the cluster RS by examining the properties of the galaxies in the CMR as predicted by our reference GALFORM model. In Fig. 9 we show a selection of the studied properties for J − K. In these plots the colour–magnitude space has been divided into pixels and the colour maps show the median value of

[2] To determine the optimized value for the slope and zero-point we provide the list of galaxy magnitudes and colours to the CURVE_FIT function in the Scientific Python library, SCIPY (http://www.scipy.org/).

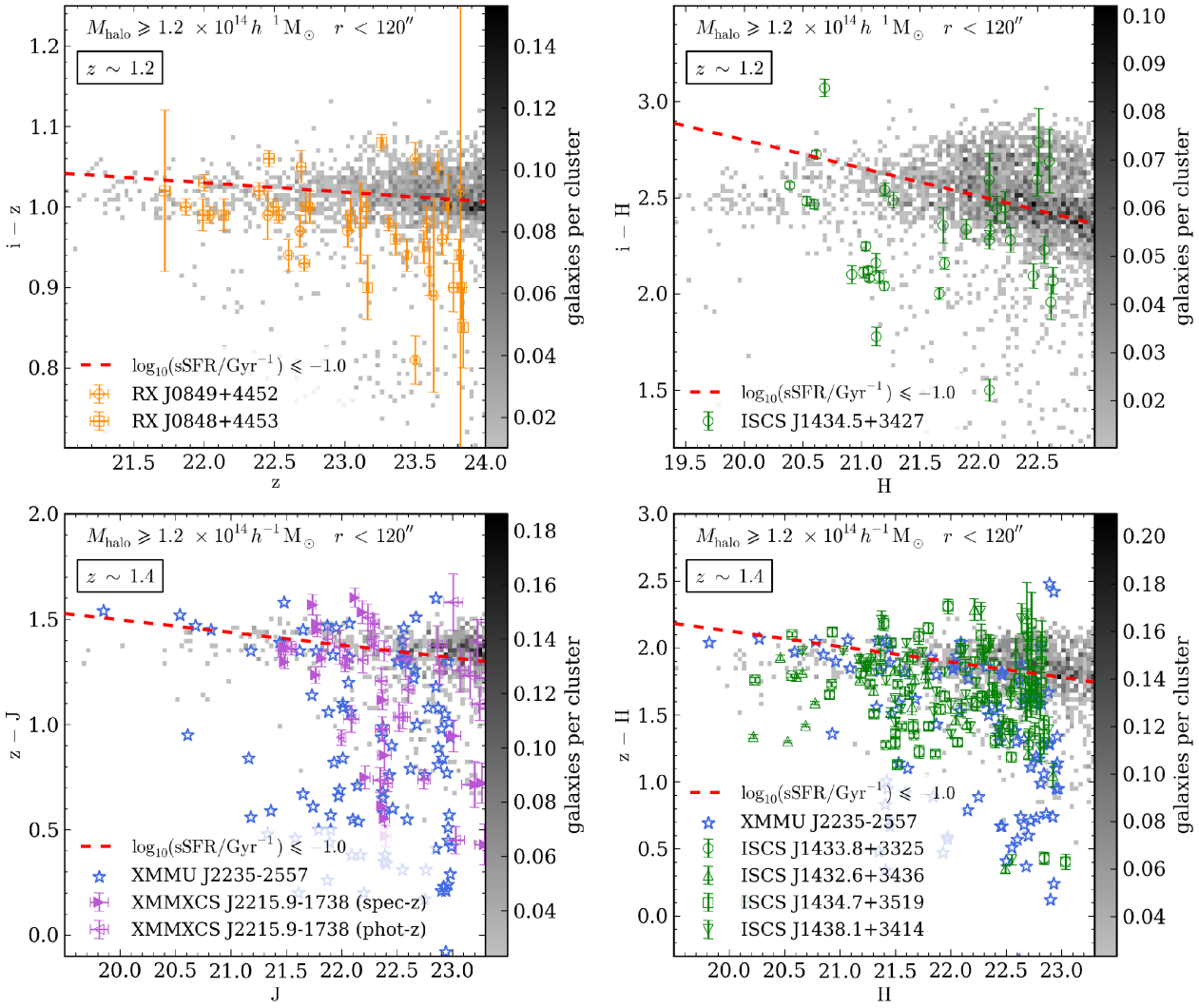

Figure 7. GALFORM CMRs at redshifts $z \sim 1.2$ (upper panels) and $z \sim 1.4$ (lower panels). The observed cluster galaxies are shown by the various data points. Grey-scale pixels show the number of cluster galaxies per cluster as predicted by the fiducial GALFORM model. The red dashed lines show linear fits to the RS predicted by GALFORM. The halo mass lower limit and aperture, r, used to select the GALFORM galaxies are shown in the label at the top of each panel.

a particular property for all of the cluster galaxies that fall in that particular pixel. We can see immediately a clear trend in galaxy properties along the RS. The upper panel of Fig. 9 shows the brightest and reddest galaxies typically having higher SFRs than faint red galaxies. The middle panel also shows that the brightest and reddest galaxies are also typically the most metal rich. Given also that these bright, red galaxies also have the largest stellar masses, this result suggests a positive correlation between stellar mass, metallicity and SFR. The existence of such a correlation between models and observations has been debated in the literature (e.g. Mannucci et al. 2010; Magrini et al. 2012; Lilly et al. 2013; Obreja et al. 2014).

In addition, the plume of bright, red galaxies that we have previously commented on is clearly evident in Fig. 9. The galaxies in the plume are revealed to typically be highly star forming (with star formation rates in excess of $1 - 10\ h^{-1}\ {\rm M}_{\odot}\ {\rm yr}^{-1}$), have reservoirs of cold gas much larger than other galaxies on the RS, be heavily attenuated by dust and have metallicities that are richer than the other galaxies on the RS. The lower panel of Fig. 9 shows the galaxies in the plume have very large optical depths, much larger than other cluster galaxies on the RS. The large dust attenuation for the galaxies in the plume would suggest that these are the same galaxies that are responsible for the discrepancy between the observed CGLF and the model prediction, though the exact cause of their large attenuation is not immediately clear. If we examine the predicted RS when we apply a weak Calzetti-like attenuation to the intrinsic magnitudes of the galaxies, then we find that the plume is removed. This happens at the expense of making the majority of bright galaxies up to one magnitude bluer, leading to a bluewards break in the bright RS. This suggests that the plume is an artefact of the model and that simply reducing the strength of the dust attenuation in the model is not an acceptable solution. Instead, this perhaps hints at an additional underlying problem in the model.

Although we suspect that the plume of star-forming galaxies in the model RS is an artefact, the scatter in the observations hints at the existence of some observed cluster galaxies with colours as red as those in the plume. Several observations of our sample of high-redshift clusters also suggest ongoing star formation activity. For the cluster XDCP J0044.0-2033, Fassbender et al. (2014) were able to obtain spectroscopic redshifts for a few galaxies with significant [O II] emission, which is often taken as an indicator for ongoing star formation. One or two of these galaxies, which we have highlighted in the bottom panel of Fig. 8, have very red J − K colours suggesting

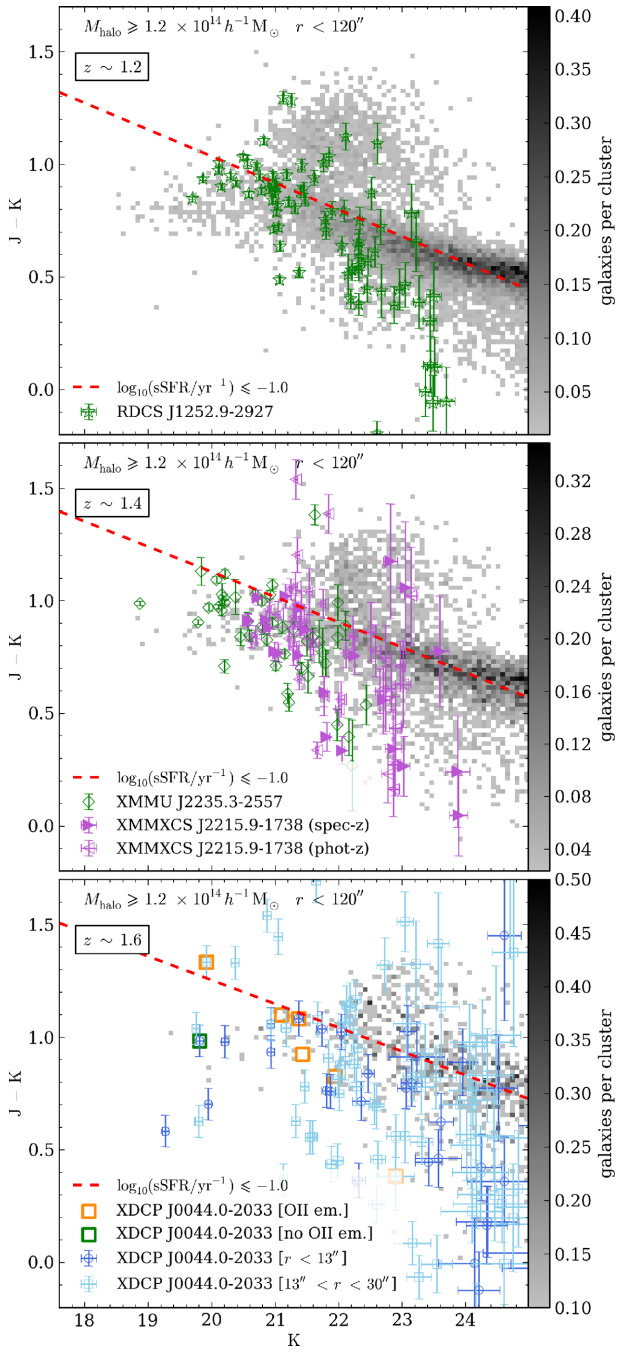

Figure 8. $J-K$ versus K CMRs for cluster galaxies at redshifts $z \sim 1.2$ (top panel), $z \sim 1.4$ (middle panel) and $z \sim 1.6$ (bottom panel). The colours of the observed galaxies are shown by the various data points. The observations at $z \sim 1.6$, from Fassbender et al. (2014), have been split according to distance r from the estimated cluster centre: galaxies within $r < 13$ arcsec (which typically have a 75 per cent membership probability) and galaxies with $13 < r < 30$ arcsec (which typically have a 50 per cent membership probability). Galaxies that have been spectroscopically confirmed are highlighted as being passive (no O II detection) or star forming (O II detection). Note that three of the spectroscopically confirmed galaxies lie at $r > 30$ arcsec. Cluster data from Hilton et al. (2009) are split into galaxies with spectroscopic redshifts (spec-z) and those without spectroscopic redshifts (photo-z). As before, the grey-scale pixels show the prediction for the fiducial GALFORM model and the red, dashed line shows the linear fit to the predicted RS. The halo mass and aperture used to select the GALFORM galaxies are shown at the top of each panel.

Table 2. Fits to the RSs predicted by the Gonzalez-Perez et al. (2014) GALFORM model for various colour–magnitude spaces between redshifts $z = 1.2$ and $z = 1.6$ using subsets of model cluster galaxies selected by a cut in sSFR (a passively evolving sample). Note that the samples were additionally limited to galaxies brighter than 25th magnitude.

Magnitude	Colour	Slope	Zero-point
Redshift: 1.2			
z	i − z	-0.0118 ± 0.0005	1.0244 ± 0.0009
H	i − H	-0.146 ± 0.002	2.436 ± 0.003
K	J − K	-0.118 ± 0.001	0.740 ± 0.002
Redshift: 1.4			
J	z − J	-0.060 ± 0.003	1.348 ± 0.004
H	z − H	-0.115 ± 0.004	1.839 ± 0.005
K	J − K	-0.112 ± 0.003	0.849 ± 0.004
Redshift: 1.6			
K	J − K	-0.106 ± 0.007	0.99 ± 0.01

such red galaxies might indeed be found in clusters in reality, though the large spread in the observations makes this unclear. Demarco et al. (2007) presented spectroscopy for the cluster of Strazzullo et al. (2006) and measured [O II] emission lines in 38 cluster members. They estimated that the SFRs of those galaxies are in the range 0.5–2 $M_\odot$ yr^{-1}, with the median SFR being $\approx$0.7 $M_\odot$ yr^{-1}. Similarly, Strazzullo et al. (2010) reported SFRs of a similar magnitude for cluster galaxies from photometry, rest-frame FUV. All of these SFR tracers suggest inferred SFRs that are not as high as the SFRs predicted by the model for those galaxies in the plume above the RS, although these SFR tracers can be heavily obscured. However measurements of near-IR spectroscopy targeting the Hα line, which is a more reliable SFR tracer, and IR photometry from *Spitzer* and *Herschel* hint to a higher SFR. For example, Valentino et al. (2015) find the Hα luminosity of cluster CL J1449+0856, at $z = 1.99$, to be significantly higher than measurements in the field at the same epoch. They attribute this to an enhanced sSFR in the cluster. In addition, based upon measurements of the Hα emission from galaxies in the Snyder et al. (2012) clusters, Zeimann et al. (2013) infer unobscured SFRs of up to 200 $M_\odot$ yr^{-1} for galaxies right down in the cluster cores. SFR measurements of the same clusters from *Spitzer* 24 μm observations, as well as *Herschel* SPIRE data, find similarly high SFRs, with the SFR in clusters increasing rapidly with redshift (Brodwin et al. 2013; Alberts et al. 2014).

6 DISCUSSION

We have seen in Section 4.2.3 that the dust attenuation calculation used in our reference GALFORM model predicts a large dust attenuation for cluster galaxies that leads to the CGLF predicted by the model being inconsistent with observations. In addition, in Section 5 we have seen that this large attenuation also produces a plume of very red galaxies above the RS, which could potentially bias predictions for the RS. We have seen that whilst applying a weaker dust attenuation removes the discrepancy between the observed CGLF and the model predictions, this leads to many of the galaxies in the RS being made too blue. Here we examine the cause of the large dust attenuation that produces the tension between the model predictions and observations.

6.1 Galaxy stellar mass–size relation

From equation (3) we can see that the dust attenuation predicted in our reference model is affected by the predicted galaxy sizes, cold

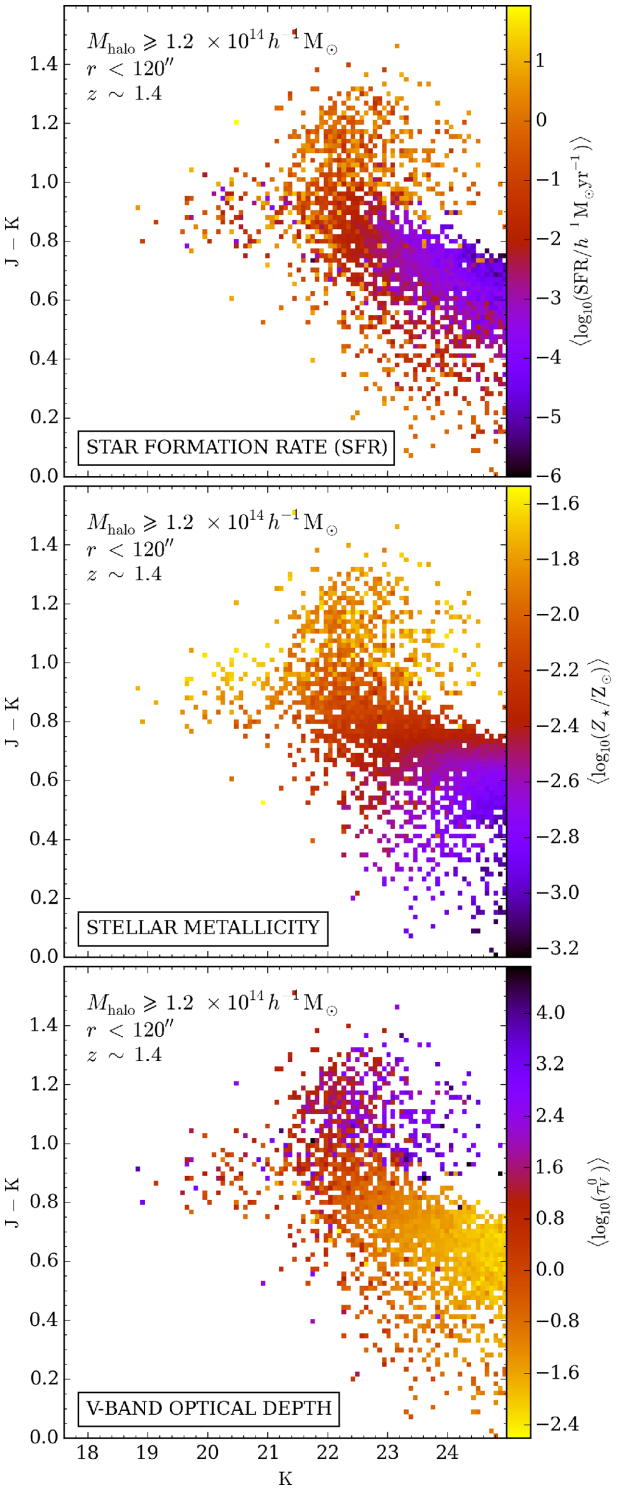

Figure 9. Distribution of various galaxy properties across the J − K versus *K* colour–magnitude space at $z \sim 1.4$. The panels, which show the distribution of star-formation rate, stellar metallicity and combined half-mass radius of the disc and bulge of the galaxies, are labelled accordingly. Each pixel is coloured according to the median value for the galaxies that lie in that pixel, with the colour scale shown at the right of each panel. The halo mass and aperture used to select the galaxies are shown at the top of each panel.

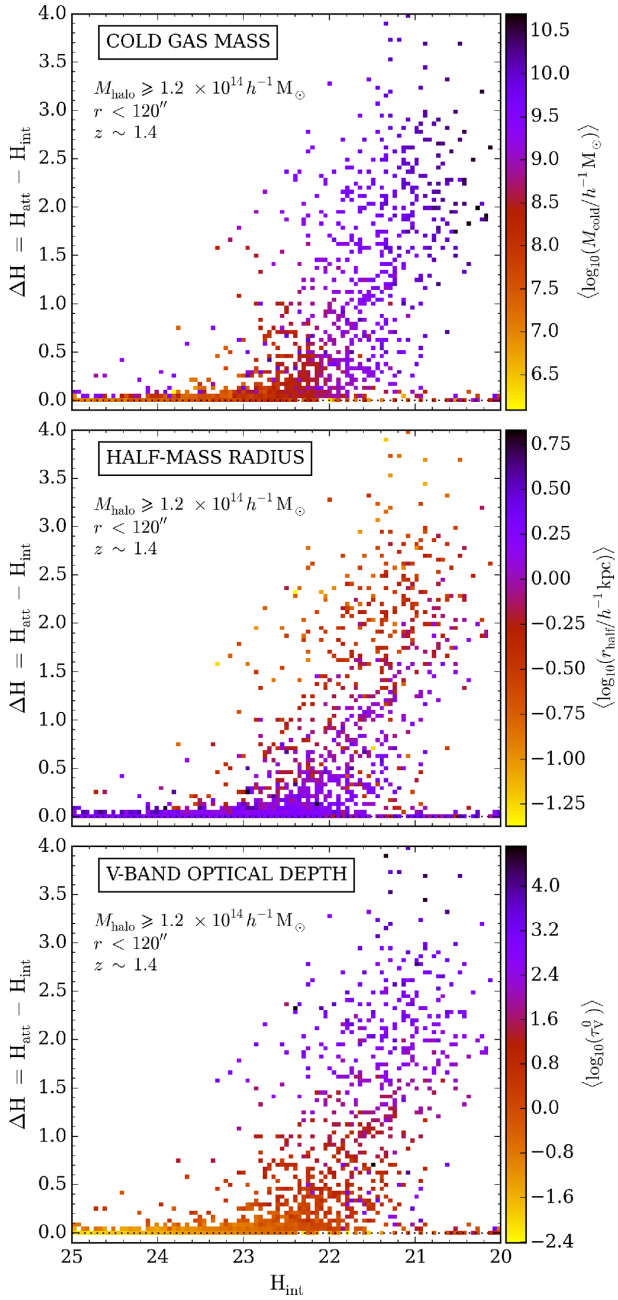

Figure 10. Difference between the H-band attenuated magnitudes and intrinsic magnitudes, as in Fig. 6, but now showing the correlation with selected galaxy properties: cold (H I, H II and He) gas mass, half-mass radius and V-band optical depth (through centre of galaxy when face-on). The pixels are coloured according to the median value of the galaxy property for the galaxies in that pixel as shown by the key on the right side of each panel. The redshift, as well as the halo mass and aperture used to select the GALFORM galaxies, are shown in each panel.

gas masses and the assumed distribution of dust with respect to stars. We have tested that changing the distribution of dust with respect to that of the galaxy stars has little impact on the CGLF. In Fig. 10 we show how selected galaxy properties change as a function of the difference between the attenuated and intrinsic H-band magnitudes of the GALFORM galaxies. We see from the bottom panel that galaxies with a large magnitude difference have a larger optical depth. We can also see that galaxies with large

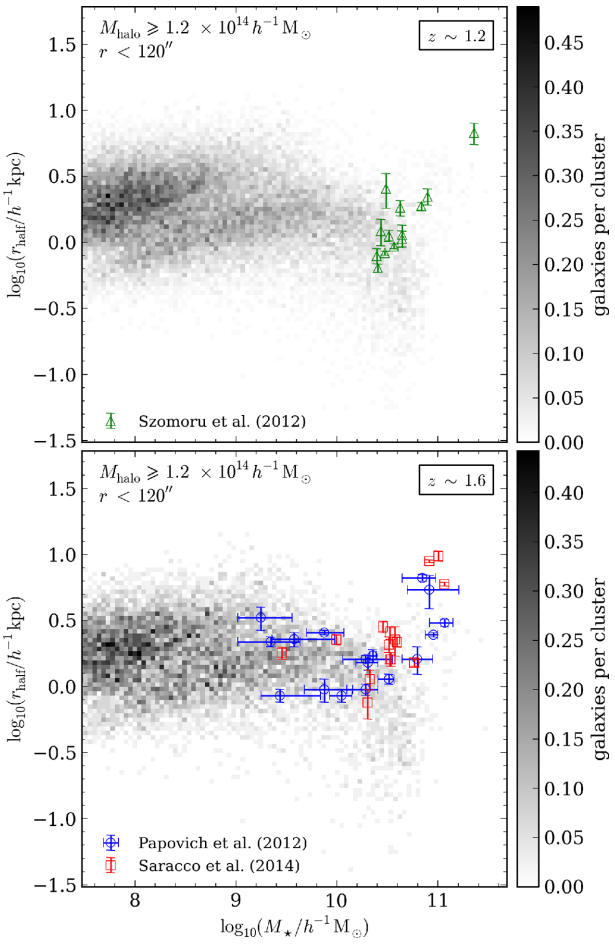

Figure 11. Comparison of the mass–size relation predicted by GALFORM, with observational measurements for high-redshift early-type galaxies made by Papovich et al. (2012), Szomoru, Franx & van Dokkum (2012) and Saracco et al. (2014). The observational estimates were converted from effective radius, $r_{\rm e}$, to half-mass radius, $r_{\rm half}$, using the conversion $r_{\rm half} = 1.35 r_{\rm e}$. The upper panel shows the model predictions and observational measurements at $z \sim 1.2$, whilst the lower panel shows the predictions and measurements at $z \sim 1.6$. The halo mass and aperture used to select the semi-analytical cluster galaxies are shown in the top-left-hand corner of each panel.

attenuation typically have larger reservoirs of cold gas and smaller radii. Both the predicted galaxy sizes and cold gas masses are fundamental predictions from the model that are directly related to the modelling of the cooling of gas and feedback processes (see Cole et al. 2000 for details of how galaxy sizes are calculated in the model). As such, directly modifying these properties is a complex procedure and beyond the scope of this paper. We do, however, in Section 6.2 briefly explore how varying selected parameters of the reference model affects the predictions for the CGLF.

Some observations at high redshift appear to be consistent with high-redshift galaxies having a small dust attenuation (e.g. Meyers et al. 2012). If we assume therefore that there is indeed negligible dust attenuation in high-redshift cluster galaxies, then from equation (3) we can see that too large an optical depth might indicate that the predicted sizes of such galaxies are too small, the amount of cold gas in the galaxies is too high or the metallicity of the cold gas is too high, or a combination of all three.

Perhaps the easiest of these properties to compare against observations is the size of the galaxies. In Fig. 11 we compare the stellar mass–size relation for the model cluster galaxies with observational estimates from Szomoru et al. (2012) at $z \sim 1.2$ and from Papovich et al. (2012) and Saracco et al. (2014) at $z \sim 1.6$. Note that the galaxies we show from Papovich et al., are those selected as cluster galaxies, whereas the galaxies from Szomoru et al., and Saracco et al., are from global samples.[3] For stellar masses $M_\star \lesssim 10^{10}\,h^{-1}\,{\rm M}_\odot$, the mass–size relation for the model, which is shown by the grey-scale pixels, is approximately flat but with a large scatter of typically 0.4–0.5 dex. The mass–size relation drops off towards the highest masses. Therefore, although there is agreement between the observations and the model predictions, the most massive cluster galaxies, with stellar masses $M_\star \gtrsim 10^{10}\,h^{-1}\,{\rm M}_\odot$, are typically smaller than the observed sizes, with some model galaxies being up to an order of magnitude smaller. Examining how the stellar mass–size relation correlates with other galaxy properties, we can see in Fig. 12 that the population of very massive, compact galaxies in the model typically have the highest optical depth, which is not surprising given equation (3). We also find that these high-mass, compact galaxies have extremely large cold gas masses of $M_{\rm cold,\,gas} \sim 10^{10}\,h^{-1}\,{\rm M}_\odot$ (comparable to their stellar masses) as well as the highest star formation rates (between $1\,h^{-1}\,{\rm M}_\odot\,{\rm yr}^{-1}$ and $10\,h^{-1}\,{\rm M}_\odot\,{\rm yr}^{-1}$).

Overall, the large reservoirs of cold gas and the compact sizes of the most massive cluster galaxies appear to be the cause of the large dust attenuation, which leads to the discrepancy between the observed CGLF and that predicted by the model. Our results therefore suggest that the problem of the large dust attenuation is actually due to an underlying problem of either the model underpredicting the sizes of the most massive cluster galaxies or the model allowing too much cooling of gas in these haloes. González et al. (2009) come to a similar conclusion when comparing predictions from the Baugh et al. (2005) and Bower et al. (2006) GALFORM models with the colours of galaxies in the Sloan Digital Sky Survey (SDSS; York et al. 2000). González et al., find that the model overpredicts the number of bright, blue galaxies and also that the bulge-dominated bright galaxies have sizes up to a factor of 10 times smaller than SDSS galaxies of equivalent luminosity. Following an examination of several of the model parameters, they attribute the problem as being due to an oversimplified treatment of the sizes of galaxy merger remnants. At lower redshift, Weinzirl et al. (2014) compare the predictions of the semi-analytical model of Neistein & Weinmann (2010) with *Hubble Space Telescope* observations of the Coma Cluster and find that the model overpredicts the mass fraction of cold gas for galaxies in haloes with Coma-like properties.

6.2 Robustness of model predictions to parameter changes

In the previous section we concluded that the discrepancy between the observed CGLF and the model predictions is likely being caused by the model predicting too much cold gas and too small sizes for the most massive cluster galaxies. Since these two fundamental galaxy properties are sensitive to many other model parameters, we

[3] To convert the stellar mass estimates from Papovich et al., and Saracco et al., from the Chabrier IMF to the Kennicutt (1983) IMF we adopt a conversion factor of −0.09 dex (Mitchell et al. 2013). To convert the stellar masses estimates of Szomoru et al., we first converted from the Kroupa (2001) IMF to the Salpeter (1955) IMF using a conversion factor of −1.6 dex (Fontana et al. 2004) and then converted from the Salpeter (1955) IMF to the Kennicutt (1983) IMF using a conversion factor of +1.4 dex (Fontana et al. 2004).

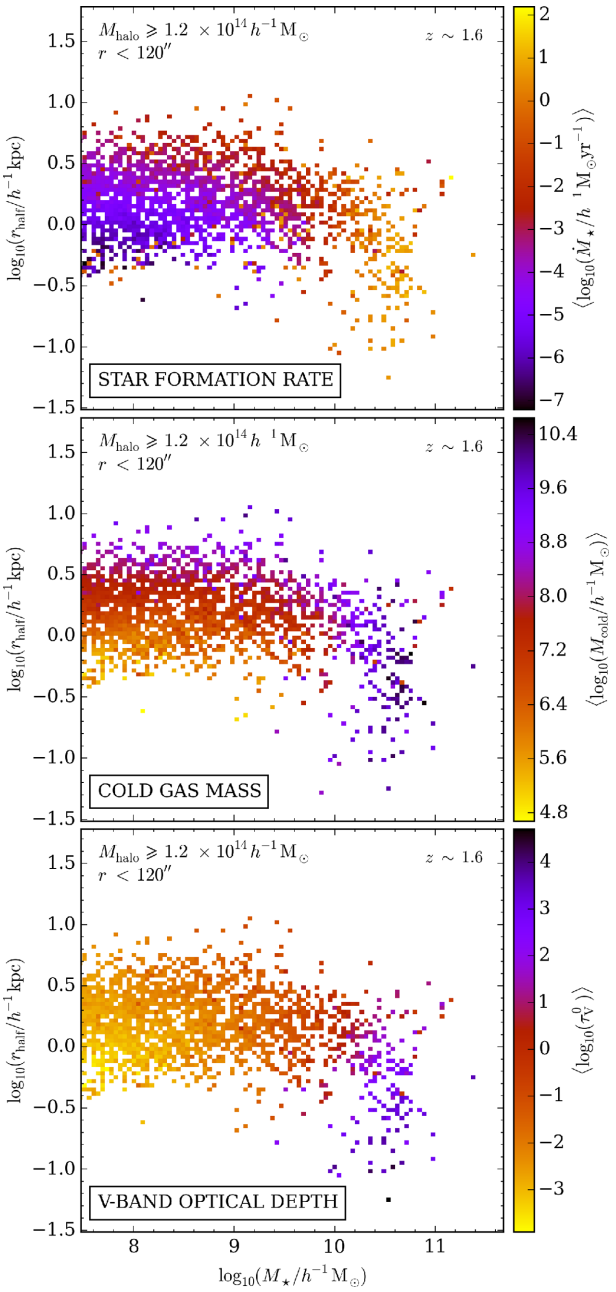

Figure 12. Distribution of selected galaxy properties along the mass–size relation as predicted by GALFORM. The various properties: star formation rate, half-mass radius and V-band optical depth, are labelled in the corresponding panel. Note that the half-mass radius includes both the disc and bulge of the galaxy and the optical depth is the depth measured through the centre of the galaxy when face-on. The pixels are coloured according to the median value of the galaxy property for the galaxies in that pixel. The redshift as well as the halo mass and aperture used to select the GALFORM galaxies, are shown in each panel.

now vary some of the key parameters that we would expect to have the greatest effect upon the high-redshift cluster galaxy population in order to gain some insight into the physics shaping the model predictions for cluster galaxies. We note that most of the parameters we choose to vary will have a greater impact on the cold gas masses of the galaxies rather than the galaxy sizes. For this exercise we will vary each parameter independently and use the prediction for the $z \sim 1.4$ CGLF as an indicator of possible improvements, since the discrepancy is most noticeable in the predictions for the CGLF. We note, however, that for a more extensive search varying multiple parameters simultaneously and examination of multiple galaxy statistics would be necessary. We leave such a search for future work.

The main parameters that we expect to have the greatest influence on the predictions for the cluster galaxy population are those governing the heating and cooling of gas in the most massive haloes as well as those parameters governing treatment of galaxy mergers. Besides these parameters, we also examined varying the scale height of the dust in the model galaxies. Although this parameter cannot improve the model predictions for the galaxy sizes or cold gas masses, it may allow an improved recovery of the CGLF. We find, however, that this has limited impact upon the model prediction for the CGLF.

6.2.1 *Galaxy mergers and interactions*

In GALFORM spheroids are created following galaxy mergers and disc instabilities. These events can also trigger starburst events, which would act to deplete the cold gas reservoirs of the merger remnant. We might expect therefore that varying the parameter governing the time-scale of these starbursts would have an effect upon the CGLF. We find, however, that changing the duration of starbursts has little impact upon the predicted CGLF.

From their analysis, González et al. (2009) found that changing the prescription for calculating the size of the stellar spheroid following a galaxy merger had a large impact upon the sizes of bright elliptical galaxies at low redshift. However, when we adopt their suggested parameter values we see little change in the CGLF or the predicted sizes for the most massive cluster galaxies. This might suggest that the amount of stellar mass produced in galaxy mergers is less important in high-redshift cluster galaxies compared to the local Universe, which agrees with the lack of sensitivity we have seen to the starburst time-scales.

Font et al. (2008) demonstrated that the incorporation of gradual ram-pressure stripping into GALFORM improves the model predictions for the colours of satellite galaxies compared with observations. Recently, Lagos et al. (2014) have also shown that gradual ram-pressure stripping is needed to reproduce the atomic and molecular gas contents of early-type galaxies. In GALFORM, when galaxies become satellites they have their hot gas stripped instantaneously. Font et al. (2008) included a prescription to delay this stripping and allowed satellite galaxies to retain a fraction of their hot gas for a longer period, thus delaying the quenching of their star formation. However, when we include the Font et al., treatment for stripping, we again see a negligible change in the prediction for the CGLF, which might suggest that the galaxy sizes are having the greatest impact upon the dust attenuation calculation.

In our reference model, the merger time-scale for a satellite galaxy is calculated, based upon dynamical friction arguments, every time its host halo undergoes a merger event. The satellite is assumed to merge on to the central galaxy after this time, irrespective of whether the sub-halo hosting the galaxy is still identifiable in the simulation. Campbell et al. (2015) recently showed that an alternative scheme, where the merger time-scale is computed once the host sub-halo can no longer be identified, leads to a change in the model predictions for the stellar mass function at $z = 0$. We find that adopting this scheme does not improve the model predictions for the CGLF.

6.2.2 *Supernovae feedback*

The amount of cold gas in massive cluster galaxies could be lowered by reducing the strength of feedback due to supernovae such that the galaxies undergo more star formation at earlier epochs, prior to them falling into the clusters. However, feedback due to supernovae is thought to affect the faint-end slope of the global galaxy luminosity function (e.g. Benson et al. 2003). As such, it is possible that reducing the strength of the supernova feedback will reduce the gas content of the galaxies, but will produce an undesirable boost in the faint end of the CGLF above the observations.

In the upper two panels of Fig. 13 we show the effect of independently varying the free parameters $\alpha_{\rm hot}$ and $v_{\rm hot}$. Variation of either parameter clearly affects the normalization of the CGLF. Understandably, the change in normalization is greater at the faint end. For the bright end of the CGLF, there is little change in the normalization as the parameters are decreased below their fiducial values, suggesting that further change in the supernova feedback alone would have minimal impact. The values for the parameters could be reduced further beyond the range considered in Fig. 13, but this would cause an excess in the faint end above the observations. As such, we conclude that changing the strength of the supernova feedback alone is unable to fix the deficit around the break in the CGLF.

6.2.3 *AGN feedback*

Feedback due to AGN is expected to have a dramatic impact on galaxies residing in relatively massive systems, like galaxy clusters, through the quenching of any active star formation.

Bower et al. (2006) and Croton et al. (2006) were amongst the first to demonstrate that introducing feedback due to AGN into semi-analytic models helps reduce the number of bright galaxies in the models, thus improving the match to the bright end of the observed global galaxy luminosity function. Additionally, the action of AGN feedback leads to the models predicting a bi-modal CMR, similar to that observed in the SDSS (González et al. 2009). Since the bright end of the global luminosity function is dominated by cluster galaxies, we expect that adjusting the parameters controlling AGN feedback will affect the predicted CGLF.

As discussed in Section 2.2, in GALFORM the strength of AGN feedback is governed by the parameter $\alpha_{\rm cool}$. The effect of varying the value of $\alpha_{\rm cool}$ on the CGLF is shown in the lower panel of Fig. 13 where we plot the H-band CGLF for a range of values of $\alpha_{\rm cool}$, either side of the value of $\alpha_{\rm cool} = 0.6$ used in the reference model. As expected, we see that variations in the value of $\alpha_{\rm cool}$ has a dramatic effect upon the sharpness of the break and normalization of the bright end of the CGLF. In contrast, the change in the normalization of the faint end of the CGLF is negligible, especially when $\alpha_{\rm cool}$ is reduced below the reference value.

We can see from Fig. 13 that reducing $\alpha_{\rm cool}$ brings the model predictions into better agreement with the observations, though even for $\alpha_{\rm cool} \lesssim 0.4$ there is still a slight discrepancy around the break in the CGLF, suggesting that a further reduction in $\alpha_{\rm cool}$ would be necessary. Examination of the CMR shows that adopting $\alpha_{\rm cool} \lesssim 0.4$ has negligible impact upon the galaxy colours, with the slope and the zero-point of the RS changing on the order of one per cent. However, as we shall see in Section 6.2.4, assuming such weak AGN feedback has a significant impact upon the model predictions at $z = 0$, which indicates that solely reducing AGN feedback is not an adequate solution and that some other mechanism must be changed,

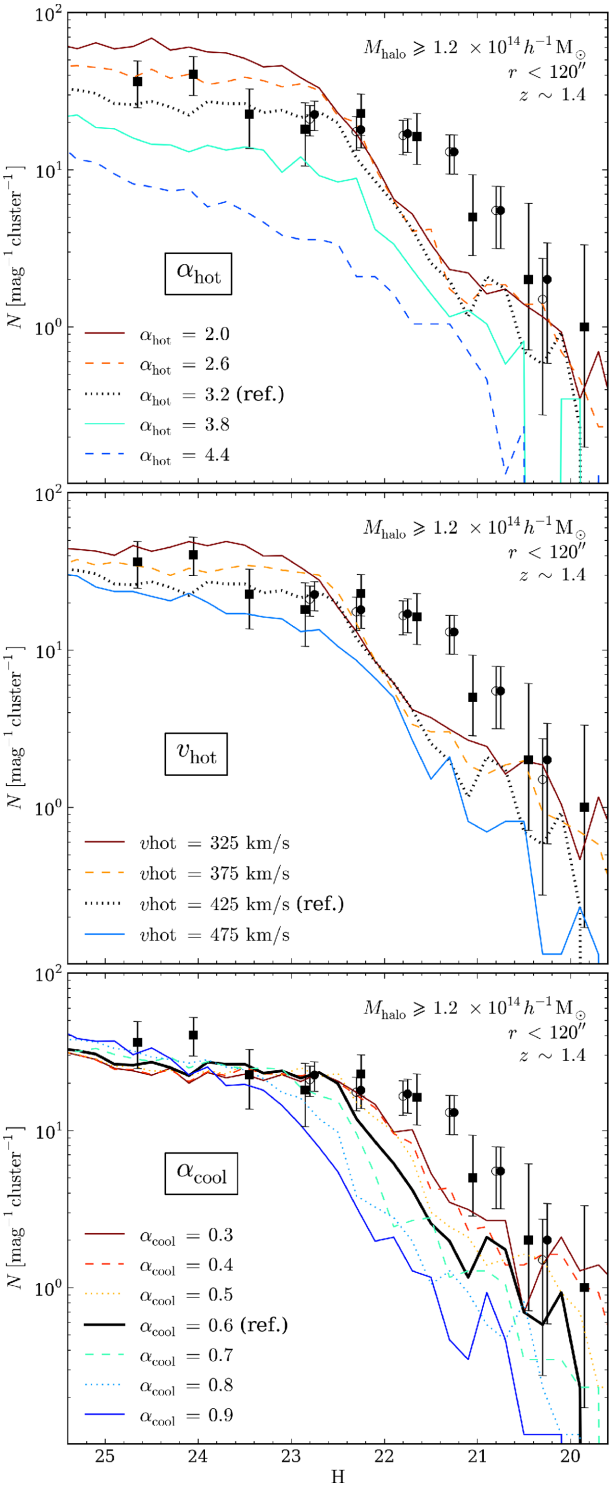

Figure 13. Impact on H-band CGLF at $z \sim 1.4$ as predicted by the GALFORM model when varying the parameters governing SN and AGN feedback. The top panel shows the predictions when varying the SN feedback parameter $\alpha_{\rm hot}$, the middle panel shows the predictions when varying the SN feedback parameter $v_{\rm hot}$ and the bottom panel shows the predictions when varying the AGN feedback parameter $\alpha_{\rm cool}$. The parameters used by our reference model are indicated in the legend of each panel. All predictions assume the dust attenuation calculation described in Section 2.3. The halo mass and aperture used to select the semi-analytical cluster galaxies are indicated in each panel. The data points are the same as from the right-hand panel of Fig. 3.

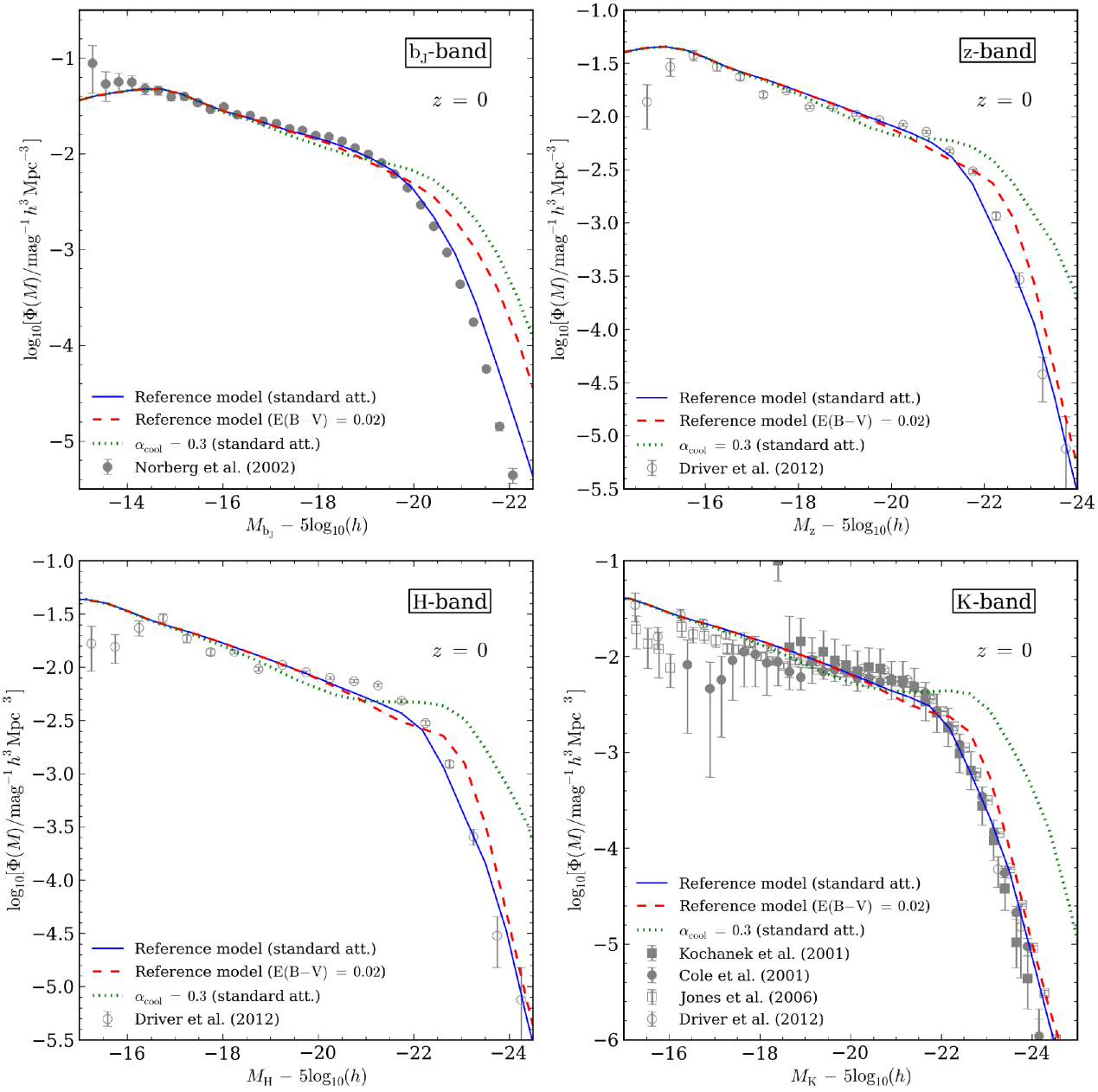

Figure 14. Predicted luminosity functions at $z = 0$ for the *global* galaxy population (both field and cluster galaxies). The panels show the luminosity functions in the b$_J$, z, H and K bands, as labelled. Data points show the observational estimates from the Two-Micron All-Sky Survey (Kochanek et al. 2001), Two-degree Field Galaxy Redshift Survey (2dFGRS; Cole et al. 2001; Norberg et al. 2002), the Six-degree Field Galaxy Survey (6dFGS; Jones et al. 2006) and the Galaxy And Mass Assembly Survey (GAMA; Driver et al. 2012). The solid blue line shows the prediction for the fiducial GALFORM model (Gonzalez-Perez et al. 2014) with the default dust attenuation calculations. The dashed line shows the prediction of the fiducial model when, instead of the default extinction, a Calzetti et al. (2000) law with E(B − V) = 0.02 is adopted. The green, dotted line shows the GALFORM prediction, with the default dust extinction, when the parameter α_{cool} is reduced from 0.6 to 0.3.

or introduced, if the model is to correctly predict the colours and abundances of high-redshift cluster galaxies.

6.2.4 *Influence on local Universe predictions*

Following our brief parameter search, we have found that the strength of AGN feedback could be used to reduce the discrepancy between the model predictions and observations of high-redshift galaxy clusters. We now examine how our attempt to match observations of high-redshift clusters changes the predictions of the model at $z = 0$, which were originally used to calibrate the model.

One of the principal statistics used to constrain the parameters of the GALFORM model is the *global* galaxy luminosity function (of both field and cluster galaxies) at $z = 0$, specifically in the b$_J$ and K bands. In Fig. 14, we show the global galaxy luminosity function at $z = 0$ for the b$_J$, z, H and K bands. The predictions for our reference GALFORM model (adopting the default dust attenuation calculation) are shown by the solid line. Since the parameters of the fiducial model have been constrained using the b$_J$- and K-band luminosity

functions, this model provides a good match to the global luminosity function in each of the four bands.

The red, dashed line in Fig. 14 shows the impact at $z = 0$ of assuming weaker dust attenuation, in this case a Calzetti et al. (2000) law with $E(B - V) = 0.02$, which gives a better match to the CGLF. As expected, weaker dust attenuation boosts the abundance of bright galaxies, with a reduction in the predicted counts around the knee of the luminosity function. The impact on the luminosity function of adopting weaker dust attenuation becomes more significant as one moves from the near-infrared towards the optical, with the K-band showing the smallest change and the b_J band showing the largest. We have seen in Section 6.2.3 that weaker AGN feedback is necessary to reconcile the model predictions for the CGLF and the observations. As such, we also plot in Fig. 14 the predicted $z = 0$ luminosity function for the model when $\alpha_{\rm cool} = 0.3$ is assumed. The effect on the luminosity function is dramatic, with the weaker AGN feedback leading to a significant excess of bright galaxies.

These latter two predictions again highlight the challenge facing current galaxy formation models. In addition to reproducing the sizes, luminosities and colours of massive galaxies in clusters, the models need to be able to remain consistent with observations of the local Universe. To achieve this requires more than one parameter to be varied as well as the possible inclusion of new physics.

7 SUMMARY AND CONCLUSIONS

We have compiled observations of high-redshift ($z > 1$) galaxy clusters, which we compare to the predictions of the Gonzalez-Perez et al. (2014) variant of the GALFORM semi-analytical galaxy formation model, which we treat as our reference model. The statistics that we consider are the CGLF and the CMR. To identify cluster galaxies in the semi-analytic catalogue, we select only those galaxies in haloes with mass greater than $1.2 \times 10^{14}\, h^{-1}\, {\rm M}_{\odot}$. We further use the distant observer approximation to apply an aperture and reject those galaxies lying further than 120 arcsec away from the halo centre.

Our reference GALFORM model predicts a CGLF in reasonable agreement with the observed CGLF at the faint and bright ends, but significantly under-predicts the number of cluster galaxies around the break in the CGLF. Examination of several possible factors that might affect the model predictions, including aperture size and halo mass selection, indicates that the discrepancy between the observations and the model predictions is likely caused by the reference model applying an overly large dust attenuation. If we instead apply a weaker dust attenuation, which we represent using a Calzetti et al. (2000) law, then the reference model prediction is able to provide a much better fit to the observed CGLF. We note that we do not advocate that a Calzetti et al., law is the correct description for dust attenuation at high redshift, but instead have simply used the law to demonstrate the impact of the large dust attenuation predicted in our reference model.

In contrast, the reference GALFORM model predicts a CMR that is qualitatively consistent with the observed colours of cluster galaxies at $z \sim 1.2$, $z \sim 1.4$ and $z \sim 1.6$. We provide linear fits to the RS for different colour-spaces using a subset of passively evolving galaxies selected using the sSFR cut, $\log_{10}({\rm sSFR/Gyr^{-1}}) \leq -1$. The slopes and zero-points of these fits are broadly consistent with observationally derived estimates.

The CMR predicted by our reference model displays a subset of very red galaxies, which appear in a 'plume' above the predicted RS. We determine that these galaxies are a result of the large dust attenuation that is causing the discrepancy between the observed CGLF and that in the model. However, although a weaker dust attenuation improves the model predictions for the CGLF, assuming a weaker dust attenuation worsens the predicted RS, with the creation of a branch of blue galaxies extending below the RS.

Examination of the properties of those galaxies with large dust attenuation reveals them to be highly star forming, with large amounts of cold gas and with small-scale sizes. The large reservoirs of cold gas and the compact sizes appear to be the cause of the large predicted dust attenuation. To gain some insight into this problem, we briefly examined how varying several key model parameters changes the predicted cluster statistics, in particular the CGLF. We find that a reduction in the strength of feedback due to AGN is able to provide some improvement in the form of the CGLF, but makes the colours of the model galaxies too blue. In addition, introducing a weaker AGN feedback significantly affects the model predictions at $z = 0$ by boosting the number of bright galaxies and over-predicting the counts at the bright end of $z = 0$ global galaxy luminosity function.

There are several possible explanations for the discrepancy between the observations and the model predictions. Amongst the most probable are that GALFORM is under-predicting the star formation of these massive cluster galaxies, or allowing too much gas cooling, which would leave them too faint (and most likely too blue) and with lots of cold gas by the time they become cluster galaxies. The problem of semi-analytical models under-predicting star formation at high redshift has been commented on several times in the literature (e.g. Daddi et al. 2007; Damen et al. 2009; Fontanot et al. 2009b; Dutton, van den Bosch & Dekel 2010; Weinmann, Neistein & Dekel 2011; Weinmann et al. 2012). Similar deficiencies have also been reported in hydrodynamical simulations (e.g. Kannan et al. 2014; Wang et al. 2015). However, it is also worth noting a recent result from Chang et al. (2015) who suggest that observational calibration of SFR estimates could be wrong by approximately a factor of two, which would result in previous observational SFR estimates being a factor of two too large. If this is the case then correcting for this would bring the observational SFR estimates and theoretical predictions into closer agreement. Additionally, the under-prediction of the sizes of the galaxies in GALFORM is likely to be having a significant impact upon the other model predictions. Predicting correct galaxy sizes is a longstanding problem for semi-analytical models since it is entangled with the contraction of the host halo. These conclusions are in agreement with previous comparisons to semi-analytical model predictions (e.g. González et al. 2009; Weinzirl et al. 2014).

Overall, these results demonstrate the challenge facing current galaxy formation models such as GALFORM: how to match the luminosity abundance and colours of cluster galaxies, whilst remaining consistent with the observed properties of galaxies in the local Universe. Achieving this will require incorporating into the models a better understanding of galaxy evolution in extreme environments. However, we must keep in mind that the comparisons in this work are limited to a small sample of individual galaxy clusters and that understanding of the astrophysical processes affecting the high-redshift galaxy population remains uncertain. Ultimately, our understanding of the abundance and properties of high-redshift clusters will only improve as we improve our statistics with up and coming deep, wide-field galaxy surveys such as DES and *Euclid*.

ACKNOWLEDGEMENTS

We thank the referee for a thorough report with many useful and constructive comments. Thanks go to Rene Fassbender, Chris

Lidman, Adam Stanford, Veronica Strazzullo and Gregory Snyder for provision of their data. In addition, we thank Begoña Ascaso, James Bartlett, Andrea Biviano, Stefano Borgani, Mark Brodwin, Alberto Cappi, Anthony Gonzalez, Sophie Maurogordato, Pierluigi Monaco, David Murphy and Adam Stanford for many useful and productive discussions and suggestions. This work was motivated by feedback from members of the Euclid Consortium Galaxy Clusters Science Working Group following the provision of galaxy mock catalogues based upon the GALFORM model. VGP acknowledges support from a European Research Council Starting Grant (DEGAS-259586). FBA acknowledges the support of the Royal Society for a University Research Fellowship. This work was carried out on the COSMA Data Centric system at Durham University, operated by the Institute for Computational Cosmology on behalf of the STFC DiRAC HPC Facility ([http://]www.dirac.ac.uk). This equipment was funded by a BIS National E-infrastructure capital grant ST/K00042X/1, DiRAC Operations grant ST/K003267/1 and Durham University. DiRAC is part of the National E-Infrastructure.

REFERENCES

Abdalla F. B., Banerji M., Lahav O., Rashkov V., 2011, MNRAS, 417, 1891
Alberts S. et al., 2014, MNRAS, 437, 437
Andreon S., Punzi G., Grado A., 2005, MNRAS, 360, 727
Angulo R. E., Springel V., White S. D. M., Jenkins A., Baugh C. M., Frenk C. S., 2012, MNRAS, 426, 2046
Ascaso B., Mei S., Benítez N., 2015, MNRAS, 453, 2515
Baldry I. K., Glazebrook K., Brinkmann J., Ivezić Ž., Lupton R. H., Nichol R. C., Szalay A. S., 2004, ApJ, 600, 681
Baugh C. M., 2006, Rep. Progress Phys., 69, 3101
Baugh C. M., 2008, Philos. Trans. R. Soc. Lond. Ser. A, 366, 4381
Baugh C. M., Lacey C. G., Frenk C. S., Granato G. L., Silva L., Bressan A., Benson A. J., Cole S., 2005, MNRAS, 356, 1191
Bell E. F. et al., 2004, ApJ, 608, 752
Benson A. J., 2010, Phys. Rep., 495, 33
Benson A. J., Bower R. G., Frenk C. S., Lacey C. G., Baugh C. M., Cole S., 2003, ApJ, 599, 38
Berlind A. A., Weinberg D. H., 2002, ApJ, 575, 587
Bower R. G., Lucey J. R., Ellis R. S., 1992a, MNRAS, 254, 601
Bower R. G., Lucey J. R., Ellis R. S., 1992b, MNRAS, 254, 589
Bower R. G., Benson A. J., Malbon R., Helly J. C., Frenk C. S., Baugh C. M., Cole S., Lacey C. G., 2006, MNRAS, 370, 645
Brammer G. B. et al., 2011, ApJ, 739, 24
Brinchmann J., Charlot S., White S. D. M., Tremonti C., Kauffmann G., Heckman T., Brinkmann J., 2004, MNRAS, 351, 1151
Brodwin M. et al., 2013, ApJ, 779, 138
Bruzual A. G., Charlot S., 1993, ApJ, 405, 538
Calzetti D., Armus L., Bohlin R. C., Kinney A. L., Koornneef J., Storchi-Bergmann T., 2000, ApJ, 533, 682
Campbell D. J. R. et al., 2015, MNRAS, 452, 852
Chabrier G., 2003, PASP, 115, 763
Chang Y.-Y., van der Wel A., da Cunha E., Rix H.-W., 2015, ApJS, 219, 8
Cole S., Lacey C. G., Baugh C. M., Frenk C. S., 2000, MNRAS, 319, 168
Cole S. et al., 2001, MNRAS, 326, 255
Croton D. J. et al., 2006, MNRAS, 365, 11
Daddi E. et al., 2007, ApJ, 670, 156
Damen M., Förster Schreiber N. M., Franx M., Labbé I., Toft S., van Dokkum P. G., Wuyts S., 2009, ApJ, 705, 617
Demarco R. et al., 2007, ApJ, 663, 164
Dickinson M., Papovich C., Ferguson H. C., Budavári T., 2003, ApJ, 587, 25
Driver S. P. et al., 2012, MNRAS, 427, 3244
Dutton A. A., van den Bosch F. C., Dekel A., 2010, MNRAS, 405, 1690
Eisenhardt P. R. M. et al., 2008, ApJ, 684, 905
Ellis R. S., Smail I., Dressler A., Couch W. J., Oemler A., Jr, Butcher H., Sharples R. M., 1997, ApJ, 483, 582
Ettori S., Tozzi P., Borgani S., Rosati P., 2004, A&A, 417, 13
Fassbender R. et al., 2014, A&A, 568, A5
Ferrara A., Bianchi S., Cimatti A., Giovanardi C., 1999, ApJS, 123, 437
Fioc M., Rocca-Volmerange B., 1999, preprint (astro-ph/9912179)
Font A. S. et al., 2008, MNRAS, 389, 1619
Fontana A. et al., 2004, A&A, 424, 23
Fontanot F., Somerville R. S., 2011, MNRAS, 416, 2962
Fontanot F., Somerville R. S., Silva L., Monaco P., Skibba R., 2009a, MNRAS, 392, 553
Fontanot F., De Lucia G., Monaco P., Somerville R. S., Santini P., 2009b, MNRAS, 397, 1776
Furlong M. et al., 2015, MNRAS, 450, 4486
Gilbank D. G., Yee H. K. C., Ellingson E., Gladders M. D., Loh Y.-S., Barrientos L. F., Barkhouse W. A., 2008, ApJ, 673, 742
Gilbank D. G., Gladders M. D., Yee H. K. C., Hsieh B. C., 2011, AJ, 141, 94
Gladders M. D., Yee H. K. C., 2000, AJ, 120, 2148
Gladders M. D., Yee H. K. C., 2005, ApJS, 157, 1
González J. E., Lacey C. G., Baugh C. M., Frenk C. S., Benson A. J., 2009, MNRAS, 397, 1254
Gonzalez-Perez V., Lacey C. G., Baugh C. M., Lagos C. D. P., Helly J., Campbell D. J. R., Mitchell P. D., 2014, MNRAS, 439, 264
Guo Q. et al., 2011, MNRAS, 413, 101
Guo Q., White S., Angulo R. E., Henriques B., Lemson G., Boylan-Kolchin M., Thomas P., Short C., 2013, MNRAS, 428, 1351
Hayashi M., Kodama T., Koyama Y., Tanaka I., Shimasaku K., Okamura S., 2010, MNRAS, 402, 1980
Hilton M. et al., 2009, ApJ, 697, 436
Hopkins A. M., 2004, ApJ, 615, 209
Huchra J. P., Geller M. J., 1982, ApJ, 257, 423
Jee M. J. et al., 2011, ApJ, 737, 59
Jiang L., Helly J. C., Cole S., Frenk C. S., 2014, MNRAS, 440, 2115
Jones D. H., Peterson B. A., Colless M., Saunders W., 2006, MNRAS, 369, 25
Kannan R., Stinson G. S., Macciò A. V., Brook C., Weinmann S. M., Wadsley J., Couchman H. M. P., 2014, MNRAS, 437, 3529
Kauffmann G. et al., 2003, MNRAS, 341, 33
Kennicutt R. C., Jr, 1983, ApJ, 272, 54
Kochanek C. S. et al., 2001, ApJ, 560, 566
Koester B. P. et al., 2007, ApJ, 660, 239
Komatsu E. et al., 2011, ApJS, 192, 18
Kravtsov A. V., Borgani S., 2012, ARA&A, 50, 353
Kriek M. et al., 2006, ApJ, 645, 44
Kriek M., van Dokkum P. G., Whitaker K. E., Labbé I., Franx M., Brammer G. B., 2011, ApJ, 743, 168
Kroupa P., 2001, MNRAS, 322, 231
Lacey C. G., Baugh C. M., Frenk C. S., Benson A. J., 2011, MNRAS, 412, 1828
Lagos C. D. P., Lacey C. G., Baugh C. M., Bower R. G., Benson A. J., 2011, MNRAS, 416, 1566
Lagos C. d. P., Bayet E., Baugh C. M., Lacey C. G., Bell T. A., Fanidakis N., Geach J. E., 2012, MNRAS, 426, 2142
Lagos C. d. P., Davis T. A., Lacey C. G., Zwaan M. A., Baugh C. M., Gonzalez-Perez V., Padilla N. D., 2014, MNRAS, 443, 1002
Laureijs R. et al. 2011, preprint (arXiv:1110.3193)
Lidman C. et al., 2008, A&A, 489, 981
Lilly S. J., Carollo C. M., Pipino A., Renzini A., Peng Y., 2013, ApJ, 772, 119
Lin L. et al., 2012, ApJ, 756, 71
López-Cruz O., Barkhouse W. A., Yee H. K. C., 2004, ApJ, 614, 679
Magrini L. et al., 2012, MNRAS, 427, 1075
Mannucci F., Cresci G., Maiolino R., Marconi A., Gnerucci A., 2010, MNRAS, 408, 2115
Marinoni C., Davis M., Newman J. A., Coil A. L., 2002, ApJ, 580, 122
Mei S. et al., 2006a, ApJ, 639, 81
Mei S. et al., 2006b, ApJ, 644, 759
Mei S. et al., 2009, ApJ, 690, 42
Mei S. et al., 2012, ApJ, 754, 141

Mei S. et al., 2015, ApJ, 804, 117
Merson A. I. et al., 2013, MNRAS, 429, 556
Meyers J. et al., 2012, ApJ, 750, 1
Miller C. J. et al., 2005, AJ, 130, 968
Mitchell P. D., Lacey C. G., Baugh C. M., Cole S., 2013, MNRAS, 435, 87
Moster B. P., Naab T., White S. D. M., 2013, MNRAS, 428, 3121
Murphy D. N. A., Geach J. E., Bower R. G., 2012, MNRAS, 420, 1861
Neistein E., Weinmann S. M., 2010, MNRAS, 405, 2717
Norberg P. et al., 2002, MNRAS, 336, 907
Obreja A., Brook C. B., Stinson G., Domínguez-Tenreiro R., Gibson B. K., Silva L., Granato G. L., 2014, MNRAS, 442, 1794
Papovich C. et al., 2012, ApJ, 750, 93
Ponman T. J., Cannon D. B., Navarro J. F., 1999, Nature, 397, 135
Romeo A. D., Napolitano N. R., Covone G., Sommer-Larsen J., Antonuccio-Delogu V., Capaccioli M., 2008, MNRAS, 389, 13
Rykoff E. S. et al., 2014, ApJ, 785, 104
Salpeter E. E., 1955, ApJ, 121, 161
Saracco P. et al., 2014, A&A, 567, A94
Schlegel D. J., Finkbeiner D. P., Davis M., 1998, ApJ, 500, 525
Smail I., Edge A. C., Ellis R. S., Blandford R. D., 1998, MNRAS, 293, 124
Snyder G. F. et al., 2012, ApJ, 756, 114
Springel V. et al., 2005, Nature, 435, 629
Stanford S. A., Eisenhardt P. R., Dickinson M., 1998, ApJ, 492, 461
Strazzullo V. et al., 2006, A&A, 450, 909
Strazzullo V. et al., 2010, A&A, 524, A17
Szomoru D., Franx M., van Dokkum P. G., 2012, ApJ, 749, 121
The Dark Energy Survey Collaboration 2005, preprint (arXiv:0510346)
Vale A., Ostriker J. P., 2004, MNRAS, 353, 189
Valentino F. et al., 2015, ApJ, 801, 132
Voit G. M., 2005, Rev. Modern Phys., 77, 207
Wang L., Dutton A. A., Stinson G. S., Macciò A. V., Penzo C., Kang X., Keller B. W., Wadsley J., 2015, MNRAS, 454, 83
Weinmann S. M., Neistein E., Dekel A., 2011, MNRAS, 417, 2737
Weinmann S. M., Pasquali A., Oppenheimer B. D., Finlator K., Mendel J. T., Crain R. A., Macciò A. V., 2012, MNRAS, 426, 2797
Weinzirl T. et al., 2014, MNRAS, 441, 3083
Williams R. J., Quadri R. F., Franx M., van Dokkum P., Labbé I., 2009, ApJ, 691, 1879
Wilson G., Muzzin A., Lacy M., FLS Survey Team 2006, in Armus L., Reach W. T., eds, ASP Conf. Ser. Vol. 357, The Spitzer Space Telescope: New Views of the Cosmos. Astron. Soc. Pac., San Francisco, p. 238
Wilson G. et al., 2009, ApJ, 698, 1943
York D. G. et al., 2000, AJ, 120, 1579
Zandivarez A., Díaz-Giménez E., Mendes de Oliveira C., Ascaso B., Benítez N., Dupke R., Sodré L., Irwin J., 2014, A&A, 561, A71
Zeimann G. R. et al., 2013, ApJ, 779, 137

This paper has been typeset from a TEX/LATEX file prepared by the author.